Boiling heat transfer in electric vehicles

Boiling Heat Transfer in Electric Vehicles

R.W. van Gils

DC 2011.52

Literature survey

Co-supervisor: M.F.M. Speetjens

Supervisor: H. Nijmeijer

Eindhoven University of Technology
Department of Mechanical Engineering
Dynamics and Control Group

Eindhoven, January 9, 2012

Contents

List of abbreviations

Acronym	Description
A/C	Air Conditioning
AC	Alternating Current
AER	All Electric Range
BEV	Battery Electric Vehicle
BJT	Bipolar Junction Transistor
CHF	Critical Heat Flux
CID	Current Interrupt Device
DC	Direct Current
ESS	Energy Storage System
EV	Electric Vehicle
FCEV	Fuel Cell Electric Vehicle
GM	General Motors
HEV	Hybrid Electric Vehicle
HVAC	Heating Ventilation Air Conditioning
HTAS	High Tech Automotive Systems
IBM	International Business Machines Corporation
ICE	Internal Combustion Engine
IGBT	Insulated Gate Bipolar Transistor
IMA	Integrated Motor Assist
kWh	kiloWatt hour
Li-ion	Lithium ion
MOSFET	Metal Oxide Semiconductor Field Effect Transistor
NiMH	Nickel Metal Hydride
PCM	Phase Change Material
PHEV	Plug-in Hybrid Electric Vehicle
PM	Permanent Magnet
PTC	Positive Temperature Coefficient
REI	Range Extender Innovations
TES	Thermal Energy Storage
TU/e	Eindhoven University of Technology
UDDS	Urban Dynamometer Driving Schedule
ZEV	Zero Emission Vehicle

1 Introduction

1.1 Background

Environmental as well as economical issues provide a compelling motive to develop clean, efficient, and sustainable vehicles for urban transportation. Automobiles constitute an integral part of our everyday life, yet the exhaust emissions of conventional internal combustion engine (ICE) vehicles are to blame for the major source of urban pollution that causes the greenhouse effect leading to global warming. Moreover, the dependence on oil as the sole source of energy for passenger vehicles has economical and political implications, and the crisis will inevitably become acute as the oil reserve of the world diminishes.

An alternative to the polluting ICE vehicles are electric vehicles (EV). Electric vehicles do not necessarily reduce the overall amount of energy used, however, this energy is no longer generated onboard, as in ICE vehicles. This energy is generated by power stations, which can use a wide variety of fuels and where the exhaust emissions can be handled responsibly. The wide range of sources for generating this electricity include, fossil fuels, nuclear power, and renewable sources such as tidal power, solar power, and wind power. This energy is then transmitted to the vehicle through use of overhead lines, wireless energy transfer such as inductive charging, or a direct connection through an electrical cable. The electricity may then be stored onboard the vehicle using a battery, flywheel, or supercapacitors. Electric vehicles enabled by high-efficiency electric motors and controllers and powered by alternative energy sources thus provide the means for a clean, efficient, and environmentally friendly urban transportation system. Since, electric vehicles have little or no emission, they have the potential to curb the pollution problem in an efficient way. Moreover, EVs are the only vehicles that have the potential to become zero-emission vehicles (ZEV) [26].

An electric vehicle (EV) is a vehicle which uses one or more electric motors for propulsion. Depending on the type of vehicle, motion may be provided by wheels or propellers driven by rotary motors, or in the case of tracked vehicles, by linear motors. Among the most widely used electric vehicles are electric bicycles and electric trains, see [36]. However, for the above described pollution problem to be decreased, the ICE cars should be replaced by electric cars. Currently, one of the main reasons for the prolongation of ICE vehicles is the range of today's electric vehicles on one battery charge. The range of these vehicles is mainly determined by the performance and cycle life of the vehicle's battery pack. The latter can be improved by thermally managing the battery pack [21]. The use of auxiliary systems such as cabin heating and air conditioning (A/C) influence the range negatively as well. This influence can be decreased by recovering waste heat for the benefit of cabin heating and implementing more efficient heat transfer methods.

1.2 EV history

Electric cars first came into existence in the mid-19th century, when electricity was among the preferred methods for automobile propulsion, providing a level of comfort and ease of operation that could not be achieved by the gasoline cars of that time. The invention of the starter motor

for the ICE vehicles, their mass production, and the inconvenience of battery charging, has resulted in the complete replacement of the electric drive by the internal combustion engine (ICE) as a propulsion method for automobiles in the early 1900s. However, electric power has remained commonplace in other vehicle types, such as trains and smaller vehicles of all types.

During the last few decades, increased concern over the environmental impact of the petroleum-based transportation infrastructure, along with the spectre of peak oil, has led to renewed interest in an electric transportation infrastructure. Vehicles making use of engines working on the principle of combustion can usually only derive their energy from a single or a few sources, usually non-renewable fossil fuels. Moreover, a key advantage of electric vehicles is regenerative braking, which allows EVs to recover energy normally lost during braking as electricity to be restored to the on-board energy storage system (ESS).

In 2003 the first mass produced hybrid gasoline-electric vehicle, the Toyota Prius, was introduced worldwide, and major auto companies have plans to introduce (plug-in) hybrid and true battery electric vehicles (BEV) in showrooms in 2010 and 2011.

On today's automobile market, several production BEVs and HEVs are available for sale or lease to the general public, such as Tesla Roadster, Ford Think City and Mitsubishi iMiEV (BEV) and Toyota Prius, Chevrolet Volt and Honda Insight (HEV). Furthermore, multiple EVs are ready to be launched in 2011 or 2012, e.g. Peugeot 106 Electric, Toyota RAV4 and Nissan Leaf (BEV) and Mercedes S400 BlueHybrid (HEV). There are also many prototype and experimental EVs being developed by the major automotive manufacturers. Most of these vehicles use Alternating Current (AC) induction motors or Permanent Magnet (PM) synchronous motors. Furthermore, almost all of these vehicles use battery technology other than the lead-acid battery pack, which ruled the battery scene for almost a century [26,32,36].

1.3 Motivation

In the 1990s the manufacturers of EVs realised that the further development of ZEV technologies was hindered by unsuitable battery technologies. Technical developments have increased the specific energy of batteries, though. Commercially available batteries such as nickel cadmium or nickel-metal-hydride can carry at best double the energy of lead acid batteries, the high temperature Sodium-nickel-chloride or Zebra battery nearly three times. However, in practice, the rechargeable battery with the highest specific energy available is the lithium polymer battery which has a specific energy about three times that of lead-acid. However, next to the fact the this type of battery is expensive, it is investigated that air cooling is insufficient for heat dissipation from large-scale batteries due to the lower thermal conductivity of the polymer [11]. Therefore, the lithium-ion battery is seen as the current best choice for EV batteries [23, 32, 46, 61]. The advantages of this technology compared to conventional NiMH batteries used to date include [23]:

- Greater performance and energy density.
- Highly compact physical dimensions.
- High charge and discharge efficiency.
- High cyclability.

Although BEVs for everyday use do not require an active thermal management scheme for optimal performance of their battery, such schemes can improve lifespan of the battery significantly. Furthermore, recovering the small amount of waste heat can be used for heating the cabin which indirectly leads to extended range per charge, as less electricity is required for heating in that case. As a reaction on the shortcomings of the battery technologies, in particular the Japanese auto industries started to develop hybrid electric vehicles (HEV). These hybrid vehicles use an electric motor and an internal combustion engine and thus do not solve the pollution problem, although it does mitigate it.

The shortcomings in lifespan of today's battery technology can be decreased by a good thermal management of EV batteries during charge and discharge procedures. As reaction times decrease and reaction resistances, power and capacity increase with temperature, unwanted reactions speed up and degrade the life of the battery faster at higher temperatures [46]. This holds for all kinds of battery technologies; lithium-ion (Li-ion), Nickel-metal-hydride (NiMH), lithium polymer batteries and lead-acid batteries, [1, 6, 32, 49, 61]. An overview of properties of these specific batteries can be found in [21, 26].

Thermal issues are of more concern in HEV pack's relative to battery electric vehicle (BEV) pack's, because of higher power and a more aggressive charge/discharge profile [48]. On the other hand the range of BEV is a crucial variable for its success, meaning the thermal management system may not use too much energy. Furthermore, the dissipated heat must be released at desired locations in order to waste as less energy as possible. The additional thermal management requirements associated with electric drive systems are also a recognized challenge in terms of costs related to the thermal management hardware, not only in terms of dollars but also in weight and size that impact the overall vehicle mass, cargo space, component packaging space and total component count [6].

1.4 Goal

As is discussed in the above, the critical component for further development of EVs is considered to be the energy storage system (ESS), which is a battery in most EVs [46]. Therefore, in this study cooling of electrical components to recover waste heat and batteries to increase lifespan in EVs is studied. The goal of this report is to gain insight in the thermal issues associated with performance of EVs in terms of range per charge and lifespan. Moreover, some of the cooling methods in today's EVs are investigated in order to place new methods in the right perspective regarding, usefulness, to what extend such cooling systems are required and to what extend the technology is really innovative. In this context also the cooling requirements of the electric motors that accelerate an EV from zero to 100 km/h in less than ten seconds are investigated.

Research will be performed on a pool-boiling model, first introduced in [16, 17, 52, 53], in order to obtain a good insight in pool-boiling phenomena. A pool-boiling system may act as physical model for heat dissipation designs based on boiling heat transfer. Such systems can be controlled by varying the sytem pressure p, which influences the critical heat flux (CHF), CHF $\propto p$, see Chapter 5. The model for pool-boiling system used here is normalised for this CHF and decreasing (increasing) the pressure thus is modelled as increasing (decreasing) the nominal heat supply Q_H, $Q_H \propto p^{-1}$. In the model stabilisation thus is to be acquired via control of a variable heat flux. This will be further discussed in Chapter 5.

The key advantages of a pool-boiling cooling scheme in EVs are (i) the reduction of weight

compared to the weight of a single-phase cooling loop, (ii) temperature uniformity of the battery in favour of battery lifespan and (iii) waste heat recovery for cabin heating. As the energy density per unit mass of the coolant is much larger than that of a single-phase cooling loop, the mass of the required coolant in the cooling design is much lower. Since boiling heat transfer occurs at a constant temperature irrespective of the heat flux, thermal management by boiling heat transfer allows for optimal temperature homogenisation of the battery. As boiling heat transfer allows for quick and intensive cooling, the removed heat can be released easily by condensation to any desired surface, for example for cabin heating.

1.5 Outline

This study is organised as follows. First in the next chapter, Chapter 2, the battery systems and cooling methods used in today's BEVs and HEVs are discussed and conclusion regarding these cooling schemes are drawn. In the subsequent chapter, Chapter 3, the power requirements of some EVs are discussed. Also the range and influence of auxiliary power requirements on range are discussed in this chapter. Then in Chapter 4 the thermal issues in EVs are discussed and in Chapter 5 a motivation for the research of pool-boiling phenomena is given. Finally, in the last chapter some conclusions are drawn.

2 Current EV's

As is mentioned in the introduction, a number of commercial, prototype, and experimental electrical vehicle models are available on today's automotive market. Almost all major automotive manufacturers produce some kind of EV or plan to do so in the near future. There are effectively six basic types of electric vehicles, [36];

1. The traditional battery electric vehicle (BEV).
2. The hybrid electric vehicle (HEV).
3. Vehicles which use replaceable fuel as the source of energy, the fuel cell electric vehicles (FCEV).
4. Vehicles supplied by power lines, e.g. trains.
5. Solar electric vehicles.
6. Vehicles that store energy in an alternative way, such as flywheels and super capacitors [21], these are almost always hybrids, using some other source of power as well.

In this Chapter only the first two types of EVs are discussed. In particular the cooling of the electrical components and batteries in BEVs and HEVs is discussed in the following two sections.

2.1 Battery electric vehicles

The type of electric vehicle that usually springs to mind when people think of electric vehicles is the battery electric vehicle. In a BEV the energy is supplied by a battery only and its propulsion mechanism solely supplied by electrical energy, making it a zero-emission vehicle (ZEV). The range per charge of these vehicles thus is solely determined by the size of the battery. Main drawback of current BEVs is the range per charge, todays battery technology can not meet the needs of todays vehicle users. Another drawback is the degredation of the batteries, after several hundreds of cycles the capacity of the battery typically decreases to 80% or less of its original capacity. If the batteries are used at elevated temperatures, this degradation even increases, see Chapter 4. A good thermal management scheme can improve lifespan and to less extend performance of EV batteries. On today's automobile market several BEVs are available, most of them use Li-ion technologies, but there are exceptions. The following BEVs are discussed hereafter:

- Tesla Roadster
- Nissan Leaf
- GM EV1
- Ford Think City
- Other BEVs

2.1.1 Tesla Roadster

The Tesla Roadster is a prototype for the high-performance BEV auto industry. The battery pack of the Tesla Roadster electric vehicle is one of the largest and technically most advanced lithium ion (Li-ion) battery packs in the world. It is capable of delivering enough power to accelerate the Tesla Roadster from 0 to 100 km/h in about 4 seconds. Meanwhile, the battery stores enough energy for the vehicle to travel more than 320 kilometres (based on EPA city/highway cycle) without recharging, something no production electric vehicle in history can claim. Details about the design of the Tesla Roadster's Li-ion battery pack is discussed in [7]. This battery pack has been under development and refinement for over three years and is the cornerstone of the Tesla Roadster.

Due to their high energy density, Li-ion batteries have become the batteries of choice in most EVs [32, 61]. However, even with this high energy density, the Li-ion batteries in the Tesla Roadster only store the energy equivalent of about 8 liters of gasoline; a very small amount of energy for a typical vehicle. The pack operates at a nominal 375 volts, stores about 53 kWh of electric energy, and delivers up to 200 kW of electric power. Due to the power and energy capabilities of the pack, safety must be considered a primary criterion in the pack's design and architecture.

The battery pack in the Tesla Roadster is comprised of about 6800 so-called 18650 cells, i.e. a small form factor battery cell of measurements of 18mm by 65mm length (hence its name). These cells are all packaged in steel cans, which provide structural rigidity and strength and offer good thermal conductivity. The dissipation of heat from a cell both extends battery life and helps maintain the pack at an even temperature. With a charge/discharge efficiency of approximately 95%, the heat generation per cycle will be approximately 2.5 kWh.

Figure 2.1 shows the complete battery pack on a cart. Note the tubes and manifold extending out of the battery pack at its lower long edge. These are used to circulate cooling fluid (a 50/50 mix of water and glycol) throughout the pack via sealed fluid paths. This enables the Roadster to keep the cells thermally balanced. This cooling system design is especially effective because thousands of small cells are combined, rather than several large ones to build an energy storage system (ESS), dramatically increasing the surface to volume ratio. Surface area is essential to cooling batteries since the surface is where heat is removed. Also, because of their small size, each cell is able to quickly redistribute heat within and shed heat to the ambient environment making it essentially isothermal. Furthermore, this cooling architecture avoids "hot spots" which can lead to failures in large battery modules.

2.1.2 Nissan Leaf

The Nissan Leaf (also formatted "LEAF" as acronym for Leading, Environmentally friendly, Affordable, Family car) is a compact 5-door hatchback electric car to be produced by Nissan. According to the manufacturer, the Leaf's all-electric range is 160 km in city driving. Sales are scheduled to begin in December 2010.

The lithium-ion battery pack holds 24kWh of energy and is rated to deliver power up to 90 kW (120 hp). The pack contains air-cooled, stacked laminar battery cells with lithium manganate cathodes. The battery pack is expected to retain 70 to 80% of its capacity after 10 years; the battery pack's lifespan depends on how often (440-volt) fast charging is used and on environmental factors such as extreme hot weather. This is the result of the thermal management system which can not dissipate the heat generated in the battery during fast

Figure 2.1: Tesla Roadster battery pack, from [7].

charging and extreme hot weather. As a result the battery temperature will rise and the battery cells will deteriorate faster as under 'normal' conditions [60].

2.1.3 GM EV1

The General Motors EV1 is an electric car that was produced and leased by the General Motors Corporation from 1996 to 1999. It is the first mass-produced and purpose-designed electric vehicle of the modern era from a major automotive industry, and the first GM car designed to be an electric vehicle from the outset. The GM EV1 models, released in 1996, use lead-acid batteries and provide the initially mediocre range of 90 to 120 km per charge. Its successor, released in 1999 has an increased range of 120 to 160 km. A fully charged battery pack containes up to 18.7 kWh for its first release with lead-acid batteries and 26.4 kWh for the second release with the NiMH batteries. The battery pack in the GM EV1 is cooled by the heating, ventilation and air conditioning (HVAC) system, meaning conditioned air is used to cool the ESS.

2.1.4 Ford Think City

The THINK City is a battery electric car with an energy efficiency of three times that of a traditional combustion engine car. The battery system of the Think can be chosen to be sodium or lithium based. Both battery systems allow for travelling up to 160 kilometers in one charge, with a top speed of 110km/h. Currently, THINK City features the Zebra sodium battery from MES-Dea and Lithium-Ion battery from EnerDel.

The Zebra (Mes-Dea) battery has a high energy density, and provides long range performance, independent of ambient temperature. It is a "hot" battery, which means that the operating temperature is between 260 and 360 degrees Centigrade. The active materials in the Zebra battery are sodium and nickel. The hot materials are contained in a vacuum insulated and sealed container, meaning these batteries operate very efficiently in areas with a very hot or a very cold climate. These batteries are thermally conditioned by a cooling plate through

which ambient air is circulated, between each second cell. The fan for cooling and an Ohmic heater for heating the battery pack, are controlled by the battery management interface for thermal management [14]. However, since this battery must be maintained at the mentioned temperature, it must be plugged in when not in use. If it is assumed that the power requirements to do this is 80W and that the car is parked for 80% of the time this will come down to a energy usage of 560 kWh per year, which seriously reduces the efficiency of these batteries.

The lithium battery operates at ambient temperatures. This means that the car does not have to be plugged in when not in use. The lithium based battery pack is supplied by EnerDel It provides the battery pack in a stacked design which provides a variety of options for cooling, which allows for optimum thermal management, performance and safety. At the Think City website no reference regarding the cooling of the Li-ion battery is provided, though [56, 58]

2.1.5 Other BEVs

Multiple experimental BEVs and converted ICE vehicles exist which have battery packs that are cooled passively by air. In most cases this leads to 10 – 20 K increase with respect to ambient temperature. Examples of ICE vehicles that are converted to BEVs are the VW Golf ECE of Essent, see [40] and the VW Lupo EL of the Eindhoven University of Technology (TU/e), see [8, 41].

2.2 Hybrid electric vehicles

A hybrid vehicle has two or more power sources, and there are a large number of possible variations. The most common types of hybrid vehicle combine an internal combustion engine with a battery and an electric motor and generator. A hybrid vehicle can either be a series, a parallel, or a series-parallel hybrid. In the former the vehicle is driven by the electromotor which is supplied with energy by the battery, by the IC driven generator unit, or by both. In the second the vehicle can either be driven by the ICE working directly through a transmission system to the wheels, by one or more electric motors, or by both. In the latter case, both the ICE and the electromotor can drive the vehicle and the electromotor can be supplied with energy by a battery and by the ICE [36, 46].

Thermal issues are of more concern in HEV battery packs relative to BEV packs, because of higher power and more aggressive charge/discharge profiles [48]. On today's market several hybrid electric vehicles are available, three of them are discussed, these are

- Chevrolet Volt
- Toyota Prius
- Honda Insight

2.2.1 Chevrolet Volt

The Chevrolet Volt (the commercial successor of the GM EV1) is an electric vehicle with a range extender, or a so-called plug-in hybrid electric vehicle (PHEV). The Volt runs on electricity from its battery and when the battery is depleted it runs on electricity created from a gas-generator, making it a series hybrid. The Volt can drive up to 64 kilometres with a

full battery, totally gas and emission free. After the 64 km, its gas-powered, range-extending generator automatically kicks in to provide electrical power.

Energy is stored on board in a 16-kWh, "t"-shaped lithium-ion battery. The battery powers the electric drive unit, which is capable of meeting full vehicle speed and acceleration performance while driving the car electrically.

The battery pack of the Chevrolet Volt is made up of more than 200 rectangular cells arranged in a series-parallel configuration. Computer systems monitor the battery cells to make sure everything is working correctly. Each battery cell is encased in a polymer coated aluminum package to withstand harsh climates. A liquid thermal cooling and heating system keeps the battery at a comfortable temperature as it is being charged and discharged [57].

2.2.2 Toyota Prius

The most well known full hybrid might be the Toyota Prius. The Prius first went on sale in Japan in 1997, making it the first mass-produced hybrid vehicle. Power to the wheels can be provided solely by a (274 Volt) Nickel Metal Hydride (NiMH) battery pack through the electric motor, directly from the gasoline engine, or from a combination of both the electric motor and the gasoline engine. The battery pack can be recharged directly by energy from the wheels powering the motor (regenerative braking) or from excess energy from the gasoline engine – which turns the generator [63]. Hence, the Toyota Prius is a series-parallel hybrid.

The Prius is equipped with a permanent magnet AC electric motor and a 274 Volt NiMH battery pack. However, there have been done some tests with Li-ion battery packs as well. the high power electric drive system and the power electronics are cooled by a (low temperature) liquid cooling loop, whereas the ICE is cooled by a separate (high temperature) cooling loop [25].

An earlier version of the Prius supplied conditioned air from the cabin as thermal management for cooling the batteries. Outside air was conditioned (heated or cooled) by the vehicle's thermal comfort system, i.e. the HVAC system, to a level comfortable for the driver. This approach has the advantage of providing air that is not only comfortable to the passenger(s), but also ideal for use in heating or cooling the NiMH batteries.

To maintain a uniform temperature distribution in the battery pack, a parallel airflow scheme was used, rather than a series configuration. In a parallel configuration, each module is set up to receive the same amount of airflow and thus the same cooling, [63].

2.2.3 Honda Insight

The Honda Insight is a parallel hybrid-electric vehicle. It is a two-seater with a lightweight aluminum body that is powered by Honda's Integrated Motor Assist (IMA) powertrain.

The Insight's IMA is powered by a flat, NiMH battery pack located below the cargo floor between the rear wheels. The 84 module battery provides a nominal system voltage of 100.8 V with a nominal capacity of 5.75 Ah. The battery is recharged automatically by scavenging engine power, when needed, and by regenerative braking when the car is decelerating. The power management electronics, battery modules, and cooling system are all self-contained within the IMA battery pack.

The battery pack temperature is conditioned by forced air. The forced air is routed from the passenger compartment to an air inlet, through the pack, and then exits the pack by being indirectly exhausted outside the car. Since the air temperature is near the passenger comfort

level, the forced air can provide a cooling effect in hotter weather and a warming effect in colder weather.

The temperature management system will attempt to accomplish two main goals: (i) maintain a reasonable temperature differential across the cells and (ii) keep the pack below a maximum temperature (usually 50-60°C for NiMH). The temperature management system comprises the fan control for air-cooling and the battery control to manage heat generation, i.e. if the battery temperature is increasing too fast, the required energy is generated by the ICE and not from the battery. In [62] this thermal management scheme is analysed. It is concluded that the thermal management scheme will only work in mild climates and not in hot temperature extremes like Arizona and cold extremes like Canada. The thermal strategy thus may seem reasonable, but if harsh conditions are encountered repeatedly, this may lead to failures and/or reduced cycle life for the battery pack. The mild management strategy will surely reduce the robustness of the pack over time [62].

2.3 Cooling schemes analysed

In the past cooling of Li-ion batteries has been an issue, see [1,61]. However, the most common type of Li-ion batteries on the market today, LiFePO4 batteries, can be cooled passively by air. Only for high performance vehicles like the Tesla Roadster the batteries require single phase liquid cooling.

As is mentioned in the foregoing, the cooling of the battery system of the Tesla Roadster is essentially isothermal. A major advantage of boiling heat transfer in this respect is that this process is isothermal as well. Furthermore this will reduce the weight of the cooling system as will discussed in Chapter 5.

The battery pack of the Nissan Leaf is actively cooled by air. However, the cooling scheme is not sufficient regarding the lifespan of the battery pack, due to short periods of elevated temperature during fast charging or hot weather. Hence, it might be concluded that more complex cooling schemes, for example single-phase liquid schemes or boiling heat transfer schemes, are required for the car to succeed on the automotive market.

The complexity of cooling schemes may be decreased by implementing a passive cooling system based on phase transition, like the pool-boiling system discussed in [16,53]. As cooling is achieved by natural convection, such system may use less energy as systems based on single-phase cooling schemes, since they require an electrical pump to circulate the coolant which reduces the allelectric range of the EVs. Moreover, as the waste heat can be recovered, it can be used to heat the cabin. In this way a boiling-based cooling scheme thus can reduce the auxiliary power requirements, increasing the all electric range as will be discussed in the next chapter.

For (P)HEVs cooling is more important as will be discussed in Chapter 4. HEVs, therefore, are more often cooled actively by single-phase cooling schemes. In HEV applications battery thermal management by boiling heat transfer thus might be interesting.

3 Energy management in EVs

In the previous chapters, BEVs and HEVs on today's automotive market are discussed. We have seen that the batteries that supply these vehicles with energy do this very efficiently and in principle can be cooled by (passive) air cooling. However, in spite of the major drawback of today's electric vehicles, i.e. their range on one charge, the energy management scheme of EVs can be improved. In many cars a large part of the battery capacity is dissipated in resistors to heat up the interior, due to which the range of the car is decreased even further [41]. In this chapter the energy management scheme of different EVs is discussed and the required energy for heating or air conditioning (A/C) is given.

3.1 Energy requirements for driving

In battery electric vehicles (BEVs) all energy required for propulsion of the vehicle is delivered by a battery pack. Main drawback of this approach is the fact that carrying energy in the form of batteries is 25 to 100 times heavier than petrol, with respect to the volume factors ranging from 10 to 40 apply. In [8] a number of BEV and equivalent ICE cars are compared. The BEVs on todays market have batteries with a capacity ranging from 16 kWh (Mitsubishi iMiev) to 53 kWh (Tesla Roadster). The battery must be able to deliver 55 to 60 kW peak power during acceleration and 10 to 20 kW continuously while driving at constant speed on a level road with a voltage of 300V or higher. Depending on the size of the battery pack these power requirements can be easily met.

In [42] a full electric 1600 kg heavy VW Golf ECE is analysed for power requirements during driving with and without auxiliary systems. Without these systems the average power consumption during city driving equals about 230 Wh/km. This can be compared with the energy consumption of the midsized PHEV vehicle in all electric range (AER) mode discussed in [47]. This vehicle has a smaller battery pack as it has a range extending ICE implemented, however, the overall vehicle mass equals 1600 kg as well. Being in AER mode, the vehicle behaves like a BEV. The energy consumption of this vehicle during the urban dynamometer driving schedule (UDDS) (city driving conditions) equals 175 - 180 Wh/km, which is of the same order of magnitude as the energy consumption of the VW Golf ECE.

The energy consumption of the VW Golf ECE at constant speed is given in Figure 3.1. For comparison the estimated energy consumption of the VW Lupo EL discussed in [8] is given in this figure as well. Note that the Lupo has an overall weight of 1030 kg, compared to the 1600 kg of the VW Golf ECE. The increased power consumption at low velocities is the result of the auxiliary power requirements of 200 W. It can be seen that the forward velocity with minimal power consumption, in spite of the auxiliary power consumption of 200 W, is about 22 km/h which is much lower than that of a diesel car.

3.2 Auxiliary energy requirements

The auxiliary power requirements of the VW Golf variant ECE are given in [42] and given in Table 3.1. If these auxiliary power requirements are compared to the average power require-

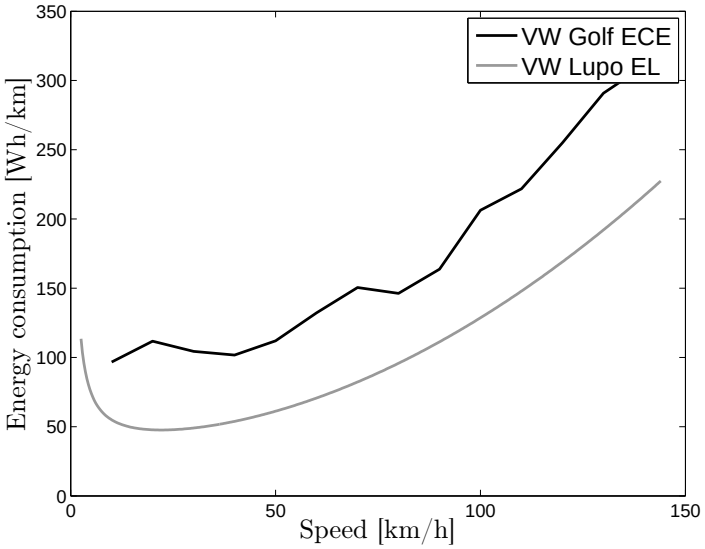

Figure 3.1: Energy consumption characteristics at constant speed, for the VW Golf ECE [42] and the VW Lupo EL [8].

ments during city driving, i.e. 9.7 kW (see [42]), then it can be considered that especially the heating and A/C systems require a large amount of the energy available from the battery. On the other hand in [8] the auxiliary power requirements are assumed to be approximately 200 W, which is a small part of the 10 kW power required for driving. This is depicted in Figure 3.2 where the energy consumption for constant speed with and without cabin heating is given. As can be seen, especially for low velocities the heating increases the energy consumption massively.

Table 3.1: Power consumption of vehicle systems and auxiliaries of the VW Golf ECE [42].

Consumer	**Power**
Vehicle systems only	0.3 kW
Vehicle systems, lights	0.5 kW
Vehicle systems, lights, heating	3.5 kW
Vehicle systems, lights, air conditioning	4.1 kW

As can be concluded from the above for urban driving, the heating and A/C, decrease the range of the vehicle significantly. In [8] the estimated driving range of the VW Lupo EL is investigated for auxiliary power requirements of 200W and 1000W, the obtained results are given in Table 3.2. As can be seen the elevated level of the auxiliary power requirements can reduce the range of the BEV with 10 to 25%. In several electric vehicles currently on the market, such as the Mitsubishi iMiev and Think City, all interior heating is provided by an auxiliary electric heater. At full power these heaters consume 3 to 4 kW. While waste heat of electric drivetrain components is relatively small compared to ICE drivetrains, the recovery of this waste heat can still significantly reduce the electric heating power required, see [41].

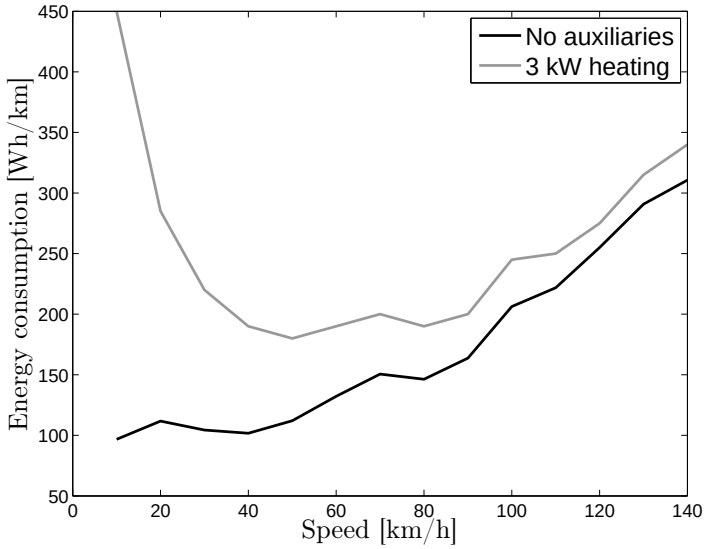

Figure 3.2: Energy consumption characteristics at constant speed, with and without heating of the VW Golf ECE [42].

Hence, replacing the electric heating by recovered waste heat can increase an EV's range, especially in urban driving, significantly. For example the discharge efficiency during a 0.5C load of 45A of LiFePo4 cells equals 95%, see [40]. This is comparable to a nominal load of 13 kW, this heat can be recovered efficienlty using boiling heat transfer.

Table 3.2: VW Lupo EL range for various driving cycles and two auxiliary power levels, from [8].

	Vehicle range [km]		**Percentage**
driving cycle	$P_{aux} = 200$ W	$P_{aux} = 1000$ W	
NEDC	214	172	80.4%
Artemis urban	212	151	71.2%
Artemis rural road	210	185	88.1%
Artemis motorway 130	138	131	94.9%
JAP 10.15	246	175	71.1%
NYCC	230	131	57.0%
UDDS/LA4	252	194	77.0%
FTP75	243	192	79.0%
LA92	193	163	84.5%
HWFET	227	205	90.3%
US06	153	142	92.8%

Finally, in [41] the range of different BEVs is considered for different auxiliary power levels, the results are depicted in Figure 3.3(a). The conclusion drawn from these results are the same

as the ones drawn in the above, i.e. auxiliary power requirements decrease range significantly.

Furthermore, it is investigated how the range of the VW Lupo EL can be increased if waste heat is recovered and used for heating the interior instead of heating the interior electrically. It is assumed that 80% of the waste heat from the inverter and motor is captured and transferred to the vehicle interior. The results of these analyses are given in Figure 3.3(b). Heat from the battery is not recovered, however, as stated in [40] this can be a significant amount of heat as well. The range thus will be increased further with waste heat recovery as depicted here.

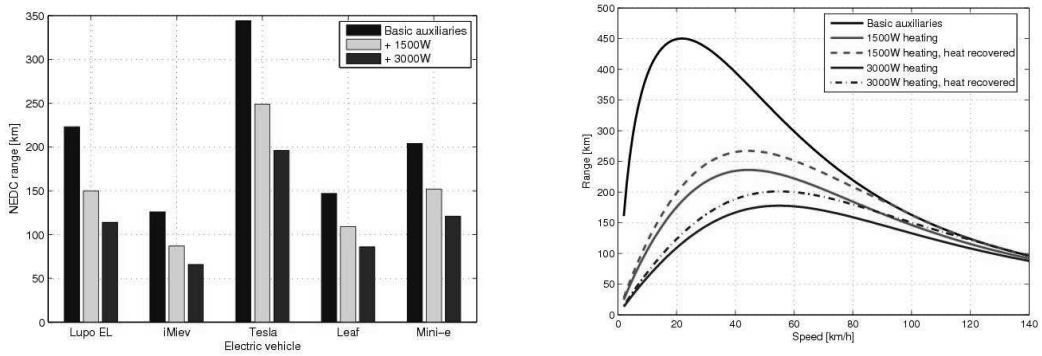

(a) NEDC cycle range

(b) VW Lupo EL

Figure 3.3: Influence of auxiliary power on range. Panel a shows the NEDC cycle range of different BEVs for different heating levels and panel b shows the range at constant speed of the VW Lupo EL and the effect of waste heat recovery, see [41].

At low speeds the use of auxiliary power has a very negative influence on the range, 3 kW heating will half the range at 50 km/h. At higher speeds this effect tones down, yet is still significant. A 3 kW electric heater reduces the range by 17% at a constant speed of 105 km/h. Utilizing all available waste heat from the motor and inverter can significantly reduce electric heating power requirements. Recovering the available waste heat, 3 kW heating power reduces the range by only 6% at a constant speed of 105 km/h. If only 2 kW of heating power would be required for the same conditions, this would have no influence on the range as the drivetrain would deliver all the heat necessary [41].

3.3 Conclusion

In this section the power requirements of common BEVs is discussed. It is found that if the battery pack is large enough it can easily deliver the 60 kW peak power required during acceleration. It is also discussed how auxiliary power requirements significantly reduce the range per charge of BEVs. Especially, the heating and A/C systems require much power. In the case of heating, this power requirement can be reduced by recovering the waste heat of battery inverter and motor.

4 Thermal Issues in EVs

In this section the thermal issues that occur in electric vehicles are discussed. To two major thermal issues are the thermal management of the battery system and the cooling scheme of the high power switching devices required for fast acceleration of the EVs.

4.1 Thermal management of the ESS

The performance and life-cycle costs of EVs depend inherently on energy storage systems (ESS) such as batteries. Battery pack performance directly affects the all-electric range, power for acceleration, fuel economy, and charge acceptance during energy recovery from regenerative braking. Because the battery pack cost, durability, and life also affect the cost and reliability of the vehicle, any parameter that affects the battery pack must be optimized. Temperature and temperature uniformity have a strong influence on battery pack lifespan and to less extend performance and consequently, that of EVs, [44, 49].

All the modules in the pack should be operated within the optimum temperature range suitable for the particular electrochemical couple used. Especially, since the optimum temperature range for the battery operation (e.g. 25°C to 45°C) is much narrower than the specified operating temperature for the vehicle (e.g. -30°C to 60°C), this can be a challenge [45].

Because HEV batteries have high specific power and undergo aggressive charging/discharging profiles, thermal issues in a HEV pack are of more concern than in BEV packs. For this reason, HEV battery packs require more effective thermal management systems like those applying boiling heat transfer.

Most of todays BEVs are equipped with Li-ion battery packs that are cooled (passively) by air. Only if the battery pack must supply a high-performance BEV like the Tesla Roadster, or fast charging schemes are used to charge the battery pack, an active thermal management scheme is required. Boiling heat transfer might be applicable in such EVs. Especially if the BEV is equipped with a large battery pack (which is necessary for an acceptable allelectric range) passive air cooling seems to suffice, however. The batteries generate a small amount of heat during normal operation and temperature only exceeds the ambient temperature by 10 – 20K [40, 42]. This does not result in decreased battery performance, however, it does accelerate cell deterioration and thermal management may in the long run thus turn out to be more effective than passive air cooling. In [50] this is investigated in terms of capacity fade of the Sony 18650 (1.8 Ah) Li-ion cells by cycling the ESS on elevated temperatures. The cells lost 31% and 36% of their initial capacity after 800 cycles at 25°C and 45°C, respectively. For a temperature of 50°C this equalled up to 50% after 600 cycles and even 70% after 500 cycles for temperatures at 55°C. Allthough, the most commonly used battery, LiFePO4 have not been subject to such analysis, analogous results might be obtained.

Next to maintaining the battery's temperature within range, another important parameter with respect to the battery performance and lifespan and thus the replacement frequency, is the module temperature uniformity, since if the cells and modules in the pack are at different temperatures, each module will be charged/discharged slightly differently during each cycle. After several cycles, modules in the pack will become unbalanced, degrading the pack's performance [48]. Hence, especially in consideration of cycle life of the battery pack a thermal

management/homogenisation scheme is indispensable. Boiling heat transfer allows for thermal homogenisation very effectively as it allows for high heat fluxes at pre-defined (constant) temperatures, as will be discussed in the next chapter. Other phase-change heat transfer applications available for thermal homogenisation is solid-liquid phase change. Solid-liquid phase change is already employed using phase-change materials (PCM) in thermal energy storage (TES) schemes in EVs [2, 33, 38]. As opposed to PCM schemes using boiling heat transfer, the consumed heat can be transported through – and released elsewhere in – the vehicle more easily. Thus enabling more efficient use of the consumed waste heat, application of TES is not possible though.

The importance of thermal management in battery packs for EV application has been an issue for all kinds of batteries. As a result a number of thermal management schemes have been investigated for all kind of battery systems. For example in [33, 38] a thermal management system that incorporates a phase change material (PCM) is considered for a Li-ion battery pack. Other heat dissipation designs for Li-ion batteries are investigated in [61]. The cooling of (valve regulated) lead-acid batteries is discussed in [37] and [5], and a water cooled nickel metal hydride (NiMH) battery system is discussed in [22].

A thermal management system may use (i) air for heating, cooling, and ventilation, (ii) liquid for cooling/heating and insulation, (iii) phase change materials for thermal storage, or a combination of these methods. Furthermore, the thermal management system may be passive (only the ambient environment is used) or active (special components provide heating and cooling at cold or hot temperatures) [45, 49].

The additional thermal management requirements associated with electric drive systems are also a recognized challenge in terms of costs related to the thermal management hardware, not only in terms of dollars but also in weight and size that impact the overall vehicle mass, cargo space, component packaging space and total component count [6].

Here the thermal management via boiling heat transfer has advantageous over PCMs and single phase liquid cooling schemes, as very little medium is required to obtain a specific heat flux due to the aggressive nature of the boiling process. Moreover, due to the passive working principle of the boiling process, the use of a bulky electric fan is no longer needed in such systems as well.

Moreover, with respect to the allelectric range of EV's it is undesirable for the A/C system to use much energy. Efficient heat transfer methods thus must be applied to cool the ambient air, see [35]. As a result, more advanced cooling schemes or heat transfer mechanisms will be used in future EVs. Such an efficient heat transfer mechanism can be based on the pool-boiling model that is investigated in [16, 52, 53], this will be discussed in Chapter 5.

4.2 Overheating of insulated gate bipolar transistors

An electrical motor drive consists of a power electronic converter an the associated controller. A power converter is made of high-power fast-acting semiconductor devices. An electric switch can change an electric circuit configuration by switching states from on to off and vice versa. The ideal switch, exhibits no voltage drop across the devices when it conducts and switches instantaneously. In practice both properties can not be reached, though.

There are several of these switches, for example the bipolar junction transistor (BJT) has high power ratings and excellent conduction characteristics, however, the base drive circuit is complicated because it is a current-driven device. The metal oxide semiconductor field

effect transistor (MOSFET) is a voltage-driven device, as a result, the gate drive circuits are much simpler. Its frequency is much higher compared to that of a BJT, however, the maximum available device power ratings would be much smaller for the former. To combine the advantageous properties of the MOSFET and the BJT, the insulated gate bipolar transistor (IGBT) has been invented. These are the devices most commonly used in EVs nowadays [26].

IGBT temperature must be maintained below a critical level. During the device, ON state, OFF state, turn-on and trun-off, a significant amount of power is produced by the flowing current and must be dissipated to the surroundings to prevent the temperature from rising to a level at which device performance is unsatisfactory or ceases altogether. In EVs the chips are required to drive electric motors, switching large amounts of power from the battery pack to electrical coils needed to accelerate the vehicle. The devices also are needed for regenerative braking; during fast charging of the battery; to convert electrical current to run accessories in the vehicle; and to convert AC to DC to charge the battery from a plug-in line. The high-power devices produce about four times as much heat as a conventional computer chip, also see [31].

To prevent overheating of IGBTs a new cooling method based on micro-channel flow boiling is proposed on the website [59]. The positive properties of micro-channel flow boiling discussed in [15] will be employed in that case. Of course boiling heat transfer is also applicable in this context. Important in this respect is that pool boiling has essential similarities with micro-channel flow boiling (relevant in many micro-fluidics applications) [27–30, 55]. Thus, these devices may also be cooled by a pool-boiling system as described in [16, 52, 53].

5 Motivation Pool-boiling project

As is demonstrated in the previous chapters, key issues in EVs are massive heat removal (of IGBTs) and thermal homogenisation (of the battery pack). Liquid-vapour phase-change heat transfer (in particular boiling) affords cooling capacities substantially beyond that of conventional methods (air/single-phase liquid cooling) and boiling heat transfer can thus improve thermal management schemes in EVs. For comparison typical heat transfer rates for forced convection by air are 0.001-0.01 W/cm^2K, for forced convection by water that is 0.1-10 W/cm^2K and boiling heat transfer by water allows for heat transfer coefficients of 0.2-200 W/cm^2K [39]. Moreover, phase-change heat transfer is an excellent way for thermal homogenisation. Phase change heat transfer occurs, independent of (local) heat-transfer rates, at a given saturation temperature and accompanying saturation pressure. Thermal homogeneity thus follows from maintaining/restoring the two-phase state at the desired temperature by regulation of the latter or, indirectly, by regulation of the pressure.

Better understanding of the dynamical behaviour of boiling and ways to control this are crucial, however. The dynamics of liquid-vapour phase-change heat transfer at solid interfaces (boiling; condensation; evaporation) can, at least in a first approach, be adequately represented by that of a pool-boiling system. The principal challenges are maximisation of heat transfer and, closely related to that, thermal homogenisation under dynamic operating conditions. These are the two key capabilities that must be strengthened in order for boiling-based thermal-management schemes to meet tomorrow's standards.

Hence, fluid boiling affords solutions to both thermal issues in EVs. Moreover, boiling has, for instance, found first applications in state-of-the-art electronics cooling systems [39] and [44]. However, thermal regulation by boiling is severely limited by the risk of "burn-out" at higher heat fluxes, see [43].

In this chapter the fundamental (pool) boiling aspects will be further discussed. Then the advantages and disadvantages of use of boiling heat transfer in EVs will be stated. Finally, the objective and strategy of the pool-boiling project mentioned in the introduction will be discussed.

5.1 Pool-boiling

Pool boiling refers to boiling heat transfer by natural convection. Pool boiling systems typically consist of a heater of which the surface is submerged in a pool of a boiling liquid. This is schematically represented in Figure 5.1. As can be seen at the bottom of the heater heat is supplied (by the to-be-cooled device) in a uniform or spatially constant fashion. This heat is then removed from the heater by the boiling liquid which as a result enters one of three possible boiling modes, i.e. nucleate boiling, transition boiling or film boiling.

Nucleate boiling is as opposed to film boiling a safe and efficient mode of heat transfer as low heater temperatures are combined with high heat transfer rates. In nucleate boiling the fluid on the heater mostly consists of liquid, however at the so-called nucleation sites, which are distributed more or less evenly over the heater surface, discrete vapour bubbles leave the heater. In film boiling on the other hand, the heater is covered by a vapour blanket. Due

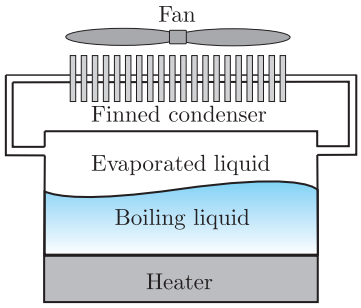

Figure 5.1: Schematical representation of a pool-boiling system.

to the insulating properties of the blanket, film boiling is accompanied by high temperatures and (relative to nucleate boiling) low heat transfer coefficients. The third mode of boiling, transition boiling, is a highly unstable mode characterised by the rapid evolution of local regions that are liquid or vapour rich. Transition boiling, unless actively stabilised, evolves towards one of the stable boiling modes, i.e. nucleate or film boiling. As a result, the transition boiling regime will only be entered during the transition form nucleate-to-film or film-to-nucleate boiling.

In pool-boiling the heat flux averaged over the heater surface, Q, is a function of the mean surface temperature, T. It is given by the global boiling curve, given in Figure 5.2. The three distinct regimes that can be observed in this boiling curve, correspond with the three fundamental boiling modes as is depicted in the figure as well. The transition nucleate-to-film boiling occurs if the heat supply Q exceeds the so-called critical heat flux (CHF), i.e. the local maximum in Figure 5.2 and thermal equilibrium is possible only in the film-boiling regime. Exceeding CHF thus triggers evolution towards film boiling and, consequently, causes significant – and, due to the risk of "burn-out" [43], potentially harmful – jumps in system temperature. This, in turn, leads to abrupt collapse of the cooling capacity and loss of the capability for thermal homogenisation at realistic operating temperatures. Thus CHF and the associated system dynamics are the key determinants for the performance of phase-change thermal-management systems. Optimal cooling performance as well as optimal thermal-homogenisation capability is a trade-off between allowing close proximity to CHF (maximum heat exchange/homogenisation range) and a safety margin (prevention of transition).

Present systems require a relatively large safety margin due to the insufficient insight into its (transitional) dynamics and ways to control it under highly-dynamic operating conditions. The potential of boiling in thermal management is therefore far from fully exploited and an increase in performance can be obtained from better control of the boiling process. Safety margins account for uncertainty in CHF (upper heat-transfer limit) and the maximum possible heat generation Q_{max}. Well-designed dynamic thermal-management schemes enable closing the gap between Q_{nom} and Q_{max}. Moreover, better prediction of (the onset to) transition boiling will reduce the safety margin on CHF, thereby further increasing this capacity.

5.2 Why pool-boiling

The key advantages of a pool-boiling cooling scheme in EVs are (i) large cooling capacities, (ii) the reduction of weight compared to the weight of a single-phase cooling loop, (iii) temperature uniformity of the battery in favour of battery lifespan and (iv) waste heat recovery for cabin

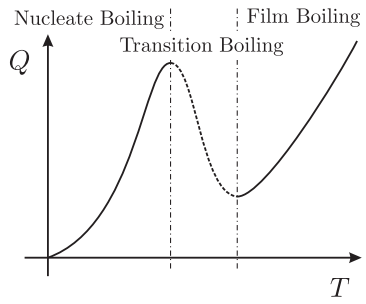

Figure 5.2: Global boiling curve

heating. To prevent the high power switching devices or IGBTs from overheating, a large heat flux per square cm is required. This can be obtained by applying boiling heat transfer to the chips. As the energy density per unit mass of the coolant is much larger than that of a single-phase cooling loop, the mass of the required coolant in the cooling design is much lower. Since boiling heat transfer occurs at a constant temperature irrespective of the heat flux, thermal management by boiling heat transfer allows for optimal temperature homogenisation of the battery. As boiling heat transfer allows for quick and intensive cooling, the removed heat can be released easily by condensation to any desired surface, for example for cabin heating.

On the other hand it is quite difficult to design a two-phase cooling loop compared to a one-phase cooling loop, as the coolant flows become turbulent by the interplay between gas and liquid. However, in [44] this problem is solved as well, so in EV application that probably is possible as well.

5.3 Objective and strategy

Aim of the proposed study is the model-based development of control strategies that safely facilitate boiling heat transfer close to CHF under dynamic operating conditions. Such control strategies are to form the basis for innovative dynamic thermal-management systems that tightly regulate the boiling process – and thus maximise cooling and thermal-homogenisation capabilities. The proposed study seeks to regulate the system pressure as a function of the (simulated) temperature distribution within the device.

The study, in a first approach, concentrates on control strategies for a basic 2D/3D pool-boiling system, see Figure 5.1 that control the stability and evolution of (heterogeneous) boiling states on the fluid-heater interface by regulating the homogeneous heat supply to the heater element as a function of the 2D/3D temperature distribution within the heater element. Here the heat supply is varied instead of the system pressure, as the model is normalised for the CHF. Note that the system pressure sets the CHF. Decreasing (increasing) p stimulates (suppresses) evaporation and thus will lead to burn-out faster (less fast). Decreasing (increasing) the pressure will thus decrease (increase) the CHF, CHF $\propto p$. Although reduction (elevation) of the pressure is accompanied by a temperature decrease (increase), the temperature distribution will remain uniform and heat flux per unit area will remain high. By regulating the pressure the system thus can be kept in the efficient nucleate boiling regime. In the model, decreasing (increasing) the system pressure is modelled by increasing (decreasing) the normalised heat supply Q_H, $Q_H \propto p^{-1}$, which will also stimulate (suppress) evaporation.

Control strategies are to be developed by means of the compact 2D/3D pool-boiling model

by [51–54]. This model leans on the phenomenological connection between the local boiling mode and the interface temperature and describes the system dynamics entirely in terms of the internal temperature distribution within the heater. As a result of which the model is called a heater-only model. The potential of this approach has been successfully demonstrated by the model-based development of a control system for boiling-curve measurements in all boiling regimes [3, 4] via the 1D model by [9, 24]. Multiple setups for control strategies with different properties for the 1D model are discussed in [16, 18]. Furthermore, first attempts to stabilise transitional states of the 2D version of the model look promising and are discussed in [17].

The principal strength of the heater-only model is that it reduces the complex boiling problem to a tractable nonlinear heat-transfer problem by establishing a one-to-one connection between the (mesoscopically)[1] local temperature and aggregation state. This enables a system-level description of pool boiling without the need to resolve microscopic (multi-phase) phenomena yet with retention of the essential heterogeneity of the transition regime. The model thus facilitates simulation of the dynamical behaviour of the entire boiling system under realistic operating conditions and therefore lends itself perfectly for the development of control strategies.

5.4 Case studies

In [19] some case studies regarding the use of a pool-boiling system to overcome thermal issues in EVs are done. Here these case studies are given as well. The model to represent the thermal management scheme is based upon the two-dimensional (2D) heater-only model first presented in [53]. In this model, the boiling fluid is solely modelled by the boundary condition on top of the heater. This can be done because of a phenomenological connection between the boiling mode and the interface temperature, cf. [53]. In the following, this model, its equilibria and the linearisation around them are discussed.

Heater-only model

In the heater-only model, the heat transfer in the 2D rectangular heater $\mathcal{H} = [0, L] \times [0, H]$ is considered – see Fig.5.3(a). The boundary segments of the heater are given by (i) adiabatic sidewalls for $x = 0$ and $x = L$, (ii) a constant heat supply extended with the system input by which unstable states must be stabilised at $y = 0$, and (iii) the nonlinear heat extraction by the boiling process on top of the heater at $y = H$.

The model describes the heat transfer in terms of the superheat $T(x, y, t)$, i.e. the temperature relative to the boiling point of the coolant. The superheat $T(x, y, t)$ within the heater is given by the heat equation

$$\frac{\partial T}{\partial t}(x, y, t) = \alpha \nabla^2 T(x, y, t), \tag{5.1}$$

[1] Here "mesoscopic" means locally averaged in space and time over intervals larger than bubble dimensions and bubble lifetimes so as to smooth out microscopic short-term fluctuations [43].

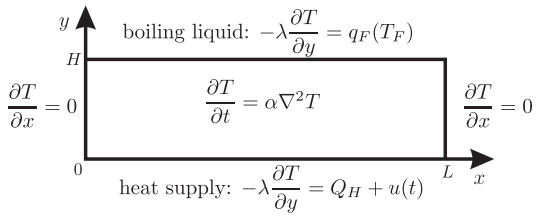

(a) Heater configuration of the pool-boiling model.

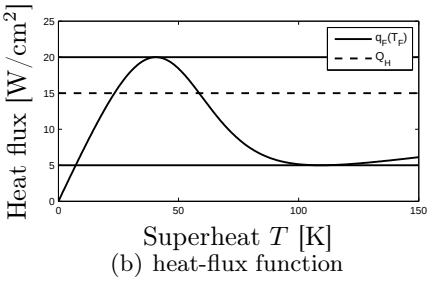

(b) heat-flux function

Figure 5.3: Heater configuration of the pool-boiling model (panel a) and nonlinear heat-flux function $q_F(T_F)$ according to the boiling curve of aluminum vs. FC-72, see [4] (panel b). The dashed line in panel b represents the nominal heat supply Q_H.

with the boundary conditions

$$\left.\frac{\partial T}{\partial x}\right|_{x=0,L} = 0, \tag{5.2}$$

$$\left.\frac{\partial T}{\partial y}\right|_{y=0} = -\frac{1}{\lambda}(Q_H + u(t)), \tag{5.3}$$

$$\left.\frac{\partial T}{\partial y}\right|_{y=H} = -\frac{1}{\lambda}q_F(T_F), \tag{5.4}$$

with $\lambda = 237\mathrm{Wm}^{-1}\mathrm{K}^{-1}$ the thermal conductivity of the aluminum heater, L its length as defined in the Introduction, H its height, $T_F := T(x, H, t)$ the fluid-heater interface temperature, $\alpha = 8.42 \cdot 10^{-5}\mathrm{m}^2/\mathrm{s}$ the thermal diffusivity of the heater, $q_F(T_F)$ the nonlinear heat flux relation given in Fig.5.3(b), $u(t)$ the system input and Q_H the nominal heat generation by the to-be-cooled device as defined in the introduction.

Burn-out is to be avoided by variation of the system pressure. Decreasing (increasing) p stimulates (suppresses) evaporation and thus will lead to burn-out faster (less fast). Decreasing (increasing) the pressure will thus decrease (increase) the CHF, i.e. the local maximum of $q_F(T_F)$ in Fig. 5.3(b), $\mathrm{CHF} \propto p$. Although reduction (elevation) of the pressure is accompanied by a temperature decrease (increase), the temperature distribution will remain uniform and heat flux per unit area will remain high. By regulating the pressure, the system thus can be kept in the efficient nucleate boiling regime. In the model, decreasing (increasing) the system pressure is modelled by increasing (decreasing) the heat supply $Q_H + u(t)$, which will lead to burn-out faster (less fast), $u(t) \propto \mathrm{CHF}^{-1} \propto p^{-1}$. As a result, the heat flux function $q_F(T_F)$ can be kept constant over time and system modelling simple.

The nonlinear heat-flux function $q_F(T_F)$ describes the *local* heat exchange between the heater and the boiling fluid as function of the *local* fluid-heater interface temperature. On physical grounds, it is identified with the so-called boiling curve, that is, the relation describing the *mean* heat exchange between heater and fluid along the *entire* fluid-heater interface (see [13]). This implies a functional relation $q_F(T_F)$ according to Fig.5.3(b). As can be seen, the function q_F comprises three distinct regimes, these correspond to one of the local boiling modes and associated boiling states: nucleate boiling (left of local maximum; fluid-rich state, efficient heat transfer), transition boiling (in between both extremes; transitional state) and film boiling (right of local minimum; vapour-rich state, inefficient heat transfer). If the heat

supply exceeds CHF, the nucleate boiling regime ceases to exist, and passing through the transition boiling regime, the film boiling regime is entered. This is accompanied with a massive increase in temperature and thus is to be avoided in practical applications.

Equilibria of the model

An extensive exposition on the steady states of this model and their stability properties is furnished in [52, 53]. Below a concise recapitulation is provided.

Steady states $T_\infty(x, y)$ of (5.1-5.4) are found via application of the method of separation of variables, see [34]. This yields a (formal) solution given by

$$T_\infty(x,y) = \sum_{k=0}^{\infty} \widetilde{T}_k \frac{\cosh(\kappa_k y)}{\cosh(\kappa_k H)} \cos(\kappa_k x) + \frac{Q_H}{\lambda}(H-y), \tag{5.5}$$

with $\kappa_k = k\pi/L$ and coefficients $\widetilde{T}_k$ the spectrum of the Fourier cosine expansion of the temperature at the fluid-heater interface,

$$T_{F,\infty}(x) := T_\infty(x,H) = \sum_{k=0}^{\infty} \widetilde{T}_k \cos(\kappa_k x). \tag{5.6}$$

These coefficients are determined by the nonlinear Neumann condition at $y = H$, upon substitution of (5.5) leading to

$$\sum_{k=0}^{\infty} \widetilde{T}_k \kappa_k \tanh(\kappa_k H)\cos(\kappa_k x) - \frac{Q_H}{\lambda} = -\frac{1}{\lambda} q_F(T_{F,\infty}), \quad \forall\, x \in [0, L]. \tag{5.7}$$

Equation (5.7) is the characteristic equation that determines the particular properties of the steady states of (5.1-5.4). If $\widetilde{T}_k = 0$ for $k > 0$, the equilibrium is constant in x-direction and (5.7) simplifies to $q_F(T_{F,\infty}) = Q_H$. As a result, $T_{F,\infty}$ coincides with the intersection(s) between the boiling curve (solid line in Fig.5.3(b)) and the nominal heat-supply (dashed line in Fig.5.3(b)). Here the left and right intersections correspond to stable nucleate and stable film boiling, respectively. The middle intersection corresponds to an unstable transition boiling equilibrium. These three equilibria are called the homogeneous equilibria as they are uniform in x-direction. All other equilibria are not uniform in x-direction and are called the heterogeneous equilibria. Heterogeneous solutions are characterised by local liquid-rich and local vapour-rich regions and thus belong to the transition boiling regime.

The principal objective here is the stabilisation of the unstable homogeneous transition equilibrium. Without stabilisation of this equilibrium, exceeding the CHF will inherently result in progression to the film boiling regime and burn-out of the to-be-cooled device. Stabilisation of this equilibrium, on the other hand, allows for increased heat flux rates and thus increases the efficiency of the cooling device. Because of the non-uniform temperature distribution of the heterogeneous equilibria, convergence towards these equilibria results in undesired non-uniform temperature distributions in the battery pack or IGBT and thus is to be avoided during operation.

Linearisation

Stabilisation of the homogeneous transition boiling equilibrium is investigated in terms of a linearisation of the pool boiling model around this equilibrium. To this end, small deviations

$v(x,y,t)$ from the equilibrium $T_\infty(x,y)$ are considered, i.e. $T(x,y,t) = T_\infty(x,y) + v(x,y,t)$. Standard linearisation methods readily yield

$$\frac{\partial v}{\partial t}(x,y,t) = \alpha \nabla^2 v(x,y,t), \tag{5.8}$$

with the boundary conditions

$$\left.\frac{\partial v}{\partial x}\right|_{x=0,L} = 0, \tag{5.9}$$

$$\left.\frac{\partial v}{\partial y}\right|_{y=0} = -\frac{1}{\lambda} u(t), \tag{5.10}$$

$$\left.\frac{\partial v}{\partial y}\right|_{y=H} = -\frac{1}{\lambda} \gamma(x) v_F(x), \tag{5.11}$$

as linear counterpart of (5.1-5.4), where $v_F(x) := v(x,H)$ and

$$\gamma(x) = \left.\frac{\mathrm{d}q_F}{\mathrm{d}T_F}\right|_{T_F(x)=T_{F,\infty}(x)}. \tag{5.12}$$

5.4.1 Control strategy

In this section, the control strategy for stabilisation of the pool boiling system is discussed. Burn-out is to be avoided by variation of the system pressure p. In order to keep the heat flux function $q_F(T_F)$ constant over time and system modelling simple, this is modelled by uniform variation $u(t)$ of the heat supply, as discussed in the previous section.

Feedback law

The intended control strategy is a feedback law based on the deviation $v(x,y,t) = T(x,y,t) - T_\infty(x,y)$ between the heater superheat $T(x,y,t)$ and its desired distribution $T_\infty(x,y)$. Easily stated, if the temperature inside the heater is lower than the desired value, $u(t)$ is positive as a result of which boiling is stimulated and lower heat fluxes are generated between heater and boiling liquid. Consequently, the device is cooled less efficient and heats itself. When the temperature is too high, the input is negative and boiling is suppressed by increasing the pressure, as a result, higher heat fluxes are generated and more heat is extracted from the device, cooling it down in the process.

The input can be calculated by evaluating the heaters temperature in only one or two specific points, however, the aim here is to evaluate the entire temperature profile in the feedback law in favor of beneficial closed-loop behaviour, i.e. the behaviour of the system with the feedback law. The heater temperature $v(x,y,t)$ is multiplied with a feedback weightfunction $g(x,y)$ to be able to give more weight to specific regions within the heater, e.g. the fluid-heater interface. As system pressure is equal in the entire boiling chamber, the system input $u(t)$ must be uniform in x-direction. As a result, the term $v(x,y,t)g(x,y)$ must be integrated over the heater domain, resulting in the feedback law

$$u(t) = \int_0^H \int_0^L v(x,y,t) g(x,y) \mathrm{d}x \mathrm{d}y. \tag{5.13}$$

This means that the controller calculates whether the overall temperature in the heater is too high or too low and stimulates or suppresses the boiling process accordingly (specific regions can be excluded or be given more weight by appropriate choice of $g(x, y)$). With the feedback weight function the properties of the feedback law, and thus the closed-loop system, will be prescribed. Furthermore, the temperature inside the heater $v(x, y, t)$ is expressed in a form that is intimately related to its natural eigenmodes. This means that in x-direction, the eigenmodes of the Laplace operator are taken to represent the profile, i.e. by a Fourier-cosine expansion. In y-direction, the profile is expressed in the non-periodic variant of this expansion, i.e. the Chebyshev expansion. This control law is discussed in full detail in [17, 20], here only a concise recapitulation is given. The temperature profile in terms of the Chebyshev-Fourier spectrum is given by

$$v(x, y, t) = \sum_{k,n=0}^{\infty} \widetilde{v}_{nk}(t)\phi_n(\theta(y))\rho_k(x), \tag{5.14}$$

with $\widetilde{v}_{nk}$ the spectral coefficients of $v(x, y, t)$, $\phi_n(\theta) = \cos(n \arccos(\theta))$ is the n-th Chebyshev polynomial, $\rho_k(x) = \cos(\kappa_k x)$ the k-th Fourier cosine polynomial and $\theta = \frac{2}{H}y - 1$ is the computational domain in y-direction, cf. [10]. Note that here an infinite series is considered, meaning no approximation error is introduced in this step. Moreover, if a smooth temperature field in the heater is assumed, due to exponential convergence of the Chebyshev-Fourier-cosine spectral coefficients, the system dynamics are mainly prescribed by the 'lower order' modes, i.e. modes with low n *and* low k. As a result, the feedback law given by (5.13) only needs to be based on these 'lower' modes, as established in [16].

In order to filter these specific modes from the profile $v(x, y, t)$, the feedback weight function $g(x, y)$ is taken as

$$g(x, y) = \sum_{q,p=0}^{\infty} \widetilde{g}_{qp}\phi_q(\theta)w_C(\theta)\rho_p(x), \tag{5.15}$$

with $w_C(\theta) = (1-\theta^2)^{-\frac{1}{2}}$ the orthogonal weight function of the Chebyshev polynomials, cf. [10] and $\widetilde{g}_{qp}$ the spectral coefficients of the weight function. Due to the orthogonality property of the Chebyshev and Fourier polynomials, implementing (5.14) and (5.15) in (5.13) reduces the feedback law to

$$u(t) = \sum_{p,q=0}^{\infty} \widetilde{v}_{qp}(t)k_{qp}, \tag{5.16}$$

where $k_{qp} = \frac{\pi H}{8}c_q c_p \widetilde{g}_{qp}$ and the factor $c_i = 2$ for $i = 0$ and $c_i = 1$ for $i > 0$, see [10].

Note that this feedback law enables control of individual Chebyshev-Fourier-cosine modes by appropriate choice of k_{qp}. This so-called modal control scheme thus enables efficient control of exactly the relevant lower order modes. Meaning that this feedback law practically is a full-state feedback, which significantly outperforms standard P-control for this boiling application [16].

The elements k_{qp} must be determined such that desired/satisfactory closed-loop dynamics are obtained. This can be done by putting the so-called closed-loop poles of the linearised system at desired/satisfactory locations. To determine these closed-loop poles, a characteristic

equation is derived analogously to the derivation of (5.7). The closed-loop poles of the system are given by the $\mu \in \mathbb{C}$ that satisfy

$$\sum_{k=0}^{\infty} A_k \rho_k(x) \left[\sqrt{\alpha_k} \tanh(\sqrt{\alpha_k} H) + \frac{1}{\lambda} \gamma(x) \right] + \sum_{k=0}^{\infty} A_k F_k \left[\frac{1}{\lambda} \gamma(x) - \sqrt{\alpha_0} \right] = 0, \tag{5.17}$$

for all $x \in [0, L]$, for nontrivial A_k (i.e. $A_k \neq 0$ for at least one k). The parameter α_k is given by

$$\alpha_k = \left(\frac{k\pi}{L} \right)^2 + \frac{\mu}{\alpha}. \tag{5.18}$$

and the closed-loop contribution F_k equals

$$F_k = \frac{\sum_{q=0}^{\infty} k_{qk} \xi_q^k}{\lambda \sqrt{\alpha_0} - \sum_{q=0}^{\infty} k_{q0} \zeta_q} \frac{e^{-\sqrt{\alpha_0} H}}{\cosh(\sqrt{\alpha_k} H)} \tag{5.19}$$

Furthermore, $(A_0 \cdots A_\infty)$ is the spectrum of the eigenmode of the closed-loop system that corresponds to the computed pole μ. The coefficients ξ^k and ζ are the spectral coefficients of the Chebyshev expansion of $\cosh\left(\sqrt{\alpha_k} \frac{H}{2}(\theta + 1)\right)$ and $e^{-\sqrt{\alpha_0} \frac{H}{2}(\theta+1)}$, respectively. Approximations to the poles of the closed-loop system can be found via discretisation of (5.17). Derivation of this expression and determination of the poles is discussed in full detail in [20].

Using this equation, the closed-loop poles for a specific feedback law, i.e. with the elements k_{nk} given, can be determined. By varying one of the elements of the feedback law, e.g. k_{00}, the poles will move away from their original position. By plotting the path the dominant poles describe as function of the controller element, a pole-trajectory plot can be obtained. Using these plots, controllers that result in satisfying closed-loop behaviour are designed.

Observer design

It is important to note that, in practical applications, the state $T(x, y, t)$ (and thus $v(x, y, t)$) can only be measured at a finite number of points on the fluid-heater interface. Therefore, the control law discussed in the above necessitates an observer or "state-estimator", see [16]. This observer estimates the temperature profile out of available measurements of the heater temperature at the measurement points.

We assume that measurements are available at $x = 0$ and $x = L$ on the fluid-heater interface, i.e. at the top left corner and the top right corner of the heater. The error between the measurements and the output of the observer is used to approximate the error $E(x, y, t)$ between system state $T(x, y, t)$ and observer state $Z(x, y, t)$, on the entire fluid-heater interface, i.e. for $y = H$, meaning $E_F^{\text{ap}} \approx E(x, H, t) = T(x, H, t) - Z(x, H, t)$. The approximation E_F^{ap} is given by the Fourier expansion of the error in the measurement points $\widetilde{x}_r = r/R$ for $r = 0, ..., R$ and $R = 1$,

$$E_F^{\text{ap}}(x) = \sum_{r=0}^{R} \frac{\eta_r}{2R} \sum_{p=0}^{R} E_F(\widetilde{x}_p) \rho_r(\widetilde{x}_p) \eta_p \rho_r(x), \tag{5.20}$$

where $\eta_i = 1$ for $i = 0 \vee K$ and $\eta_i = 2$ for $0 < i < K$. As observer we employ a copy of the nonlinear system with injection of E_F^{ap} on the boundary segment where the measurements are available, i.e. at the fluid-heater interface.

The observer thus is governed by

$$\frac{\partial Z}{\partial t}(x, y, t) = \alpha \nabla^2 Z(x, y, t), \tag{5.21}$$

with the boundary conditions

$$\left.\frac{\partial Z}{\partial x}\right|_{x=0,L} = 0, \tag{5.22}$$

$$\left.\frac{\partial Z}{\partial y}\right|_{y=0} = -\frac{1}{\lambda}(Q_H + u(t)), \tag{5.23}$$

$$\left.\frac{\partial Z}{\partial y}\right|_{y=H} = -\frac{1}{\lambda} q_F(Z_F) + q E_F^{ap}(x), \tag{5.24}$$

where q is the observer gain by which the observer error dynamics must be stabilised. Local stability of the observer error dynamics can be guaranteed via analysis according to (5.17) of the linearised observer error dynamics.

Controller-observer combination

The stability of the closed-loop system is only guaranteed in a small region around the to-be-stabilised equilibrium (local asymptotic stability) as it is based on the linearisation of the nonlinear system and observer. The so-called region of attraction of the closed-loop system, i.e. the region in which initial states converge to the equilibrium, can not be determined, however. In the next section simulations are performed and it will be shown that in some cases this region of attraction can be quite large. For some heater heights it is not possible to stabilise the homogeneous transition boiling equilibrium and, although the observer state converges to the system state in those cases, the system state converges to a non-uniform (and therefore undesired) temperature profile.

5.4.2 Closed-loop Simulations

To determine the effectiveness of the control strategy discussed in the previous section, some simulations are done with the unstable transition towards film boiling is stabilised. It turns out that this transition state can only be stabilised for specific combinations of the heater properties λ (heater material) and L, H (heater dimensions), for given Q_H (nominal heat supply). This means that in the design of a thermal management system for EVs, it is important to determine the typical value for the heat generation Q_H and choose heater dimensions and material accordingly.

In the following, two case studies are discussed. The first represents the design of a cooling device for IGBTs and the second a thermal management and homogenisation scheme for a small battery cell. As the pressure can be varied only within a certain operating range, the input is restricted by $-0.8Q_H \leq u(t) \leq 2Q_H \; \forall \; t > 0$ in the simulations.

For the simulations, discretisation of the nonlinear system is accomplished by a Chebyshev-Fourier-cosine spectral method identical to that underlying (5.14) in combination with a second-order Cranck-Nicholson time-marching scheme [10]. This admits a highly accurate

approximation of the underlying nonlinear PDE with reasonable finite resolutions. The discretised system is then solved for each Fourier-mode individually; their coupling via the boundary condition on $y = H$ is treated by a standard Picard iteration [34]. The initial conditions are constructed similarly as in [16]: $\widetilde{\boldsymbol{T}}(0) = \widetilde{\boldsymbol{T}}_\infty + \epsilon \boldsymbol{n}$, with $\widetilde{\boldsymbol{T}}_\infty$ the to-be-stabilised equilibrium and $\epsilon \boldsymbol{n}$ an exponentially-decaying Gaussian perturbation (standard deviation equals 1) with magnitude ϵ. In the following $\epsilon = 10^{-1}$ is taken.

IGBT-cooling

IGBTs are high-power switching devices used to switch large amounts of power from the battery pack to electrical coils, which produce about four times as much heat as a conventional computer chip. For this case study the heat generation Q_H is set to $Q_H = 15$ W/cm^2 see also [12]. For two different heater designs, i.e. the height of the heater is varied, the control strategy introduced above is applied to the system for stabilisation of the homogeneous transition state. It will be shown that the heater can not be made too thin as this promotes non-uniform temperature distributions in the device. The length of the heater in this case is $L = 80$mm, which is the length of an IGBT of dimensions 80×80mm.

Heater height: $H = 20$mm

The controller and observer parameters are taken according to

$$\begin{aligned}(k_{0,0}, k_{1,0}, k_{2,0}) &= (-30, -10, 6.6),\\ q &= 2,\end{aligned} \tag{5.25}$$

and controller parameters for higher Fourier-Chebyshev modes, i.e. k_{nk} for $n > 3$ or $k > 0$, equal zero. In Fig.5.4(a) the simulated evolution of the interface temperature ($T_F(x,t) := T(x,H,t)$) is shown (progression in time is indicated by darker shades of grey of the intermediate profiles). This reveals a smooth progression from an essentially heterogeneous initial state, to the final homogeneous state. This means that disturbances that arise during operation can be suppressed effectively, resulting in constant and uniform temperatures. As can be seen the region of attraction is quite large in this case. Although the temperature of the IGBT is too high initially, the controller manages to remove the excess heat in the IGBT and the heater. As a result, the superheat drops to the desired value of 60K. Fig. 5.4(a) shows that the initial temperature fluctuations in x-direction are rapidly smoothed out, resulting in a homogeneous temperature distribution in the device.

The temperature as function of time in the points $(x,y) = (0,H)$, $(x,y) = (\frac{1}{2}L, H)$ and $(x,y) = (L,H)$, i.e. the validation points, of both system and observer is given in Fig. 5.4(b). It can be seen that the observer state quite rapidly converges to the system state, from whereon the system state converges to the equilibrium.

Finally, the input used to stabilise the equilibrium is given as function of time in Fig. 5.5. Initially, the input is maximal due to the observers initial state, subsequently, the input is minimal until the temperature setpoint is reached.

Heater height: $H = 8$mm

If the heater is $H = 8$mm of height, the transition to film boiling can not be stabilised, since the interface temperature converges to a non-uniform state (partial vapour blanket). The

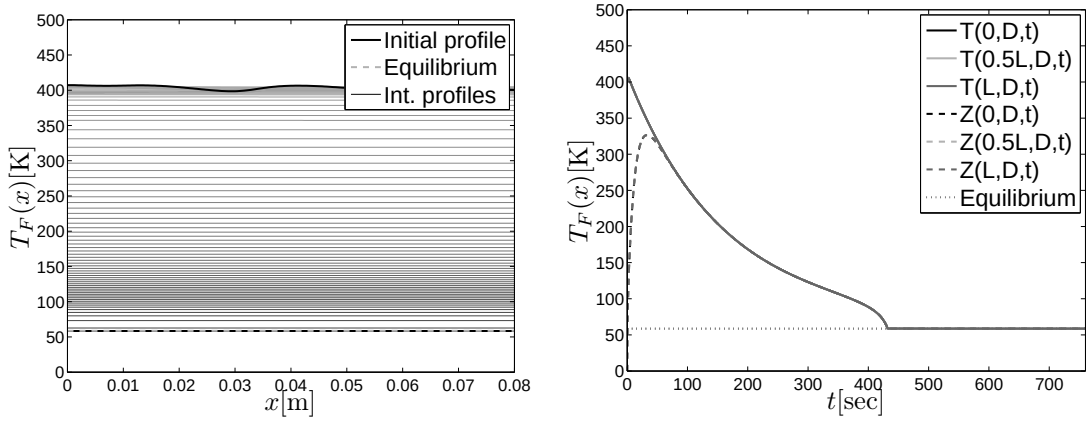

(a) Evolution of T_F as function of x

(b) Evolution of T_F as function of t

Figure 5.4: The evolution of the interface temperature $T_F(x,t)$ is shown for the IGBT-cooling case study, $H = 20$mm. The thin grey lines (in panel a) are intermediate profiles, progression in time is indicated by darker shades of grey. In panel b the evolution in the points $x = 0$, $x = \frac{1}{2}L$ and $x = L$ is shown for the system (solid line) and the observer (dashed line).

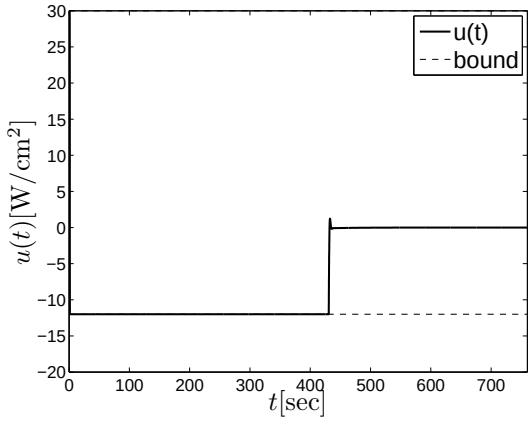

Figure 5.5: The input as function of time is shown for the IGBT-cooling case study, $H = 20$mm. The bounds of the input are given by the dashed lines.

controller and observer parameters are taken according to (5.25). The non-uniform state has temperatures that correspond to film boiling and regions with temperatures that correspond to nucleate boiling. The device thus will get very hot in some regions, while other regions still are well cooled. This phenomenon can not be avoided by taking different controller parameters as the homogeneous transition equilibrium is non-stabilisable for these system parameters. As the pressure can not be altered as function of x, the heat supply in our model must be varied uniformly. As a result, the system is not fully controllable. Depending on the system parameters the homogeneous transition equilibrium is then either stabilisable or non-stabilisable. In Fig. 5.6(a) the evolution of the fluid-heater interface temperature is shown. Although the initial condition is taken quite close the the equilibrium, the small perturbations are amplified by the boiling process resulting in the non-uniform temperature distribution.

This results in a large temperature distribution in the device.

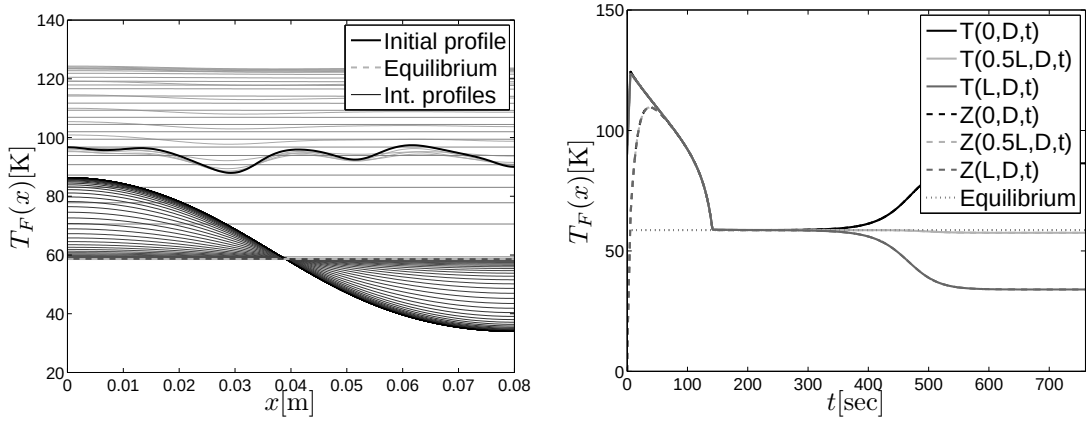

(a) Evolution of T_F as function of x

(b) Evolution of T_F as function of t

Figure 5.6: The evolution of the interface temperature $T_F(x,t)$ is shown for the IGBT-cooling case study, $H = 8$mm. The thin grey lines (in panel a) are intermediate profiles, progression in time is indicated by darker shades of grey. In panel b the evolution in the points $x = 0$, $x = \frac{1}{2}L$ and $x = L$ is shown for the system (solid line) and the observer (dashed line).

In Fig. 5.6(b) the evolution of the system and observer state in the validation points is given. Initially the observer state has a large deviation from the system state. As a result, the system state is regulated in opposite direction initially. After the observer state has converged on the system state, the system state is regulated towards the equilibrium. The non-uniformity thus is not the result of poor observer performance. After some time the system state starts to deviate from the equilibrium and convergence to a non-uniform state is observed.

In Fig. 5.7 the input as function of time is given. It can be seen that the input settles at a nonzero value after the system state has converged on the non-uniform state.

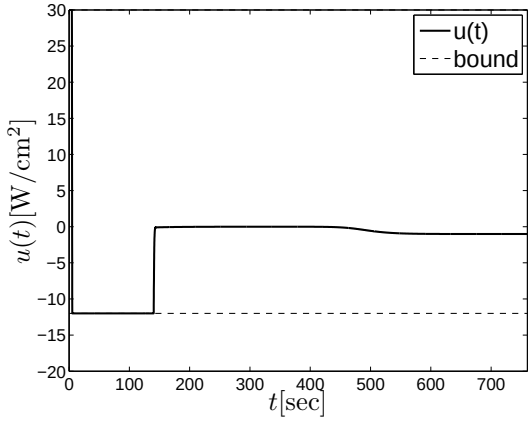

Figure 5.7: The input as function of time is shown for the IGBT-cooling case study, $H = 8$mm. The bounds of the input are given by the dashed lines.

In some cases, the convergence on the non-uniform state can be remedied by varying the

nominal pressure p (thus creating another equilibrium to stabilise). However, for these heater properties the only measure that can be taken, is a large safety margin between actual heat flux and critical heat flux (CHF). This will adversely affect the cooling efficiency, though.

Battery thermal management

The second case study is the thermal homogenisation of a small battery cell, like for example used in the Tesla Roadster. The same setup (Fig. 5.1) is used as thermal management scheme. Since the cells are closely packed together in a battery pack, the boiling chamber becomes very confined, thus significantly limiting the amount of boiling liquid. As a result, the net evaporation/condensation of the total amount of working fluid plays a significant role in the cooling process. Physical considerations suggest that in a first approximation this can be described by rescaling the boiling curve. The critical heat flux (CHF) will namely effectively decrease if the volume of the liquid phase of the boiling medium drops below a certain minimum due to net evaporation of the total amount of working fluid. For this case study the boiling curve given in Fig. 5.8 therefore is taken. The battery pack in the Tesla Roadster can deliver up to 200 kW of electric power at 95% efficiency, see [7]. This means the heat generation of an individual battery cell can be as high as approximately 0.33 W/cm^2. Hence, the heat generation is set to $Q_H = 0.33\text{W/cm}^2$ for this case study.

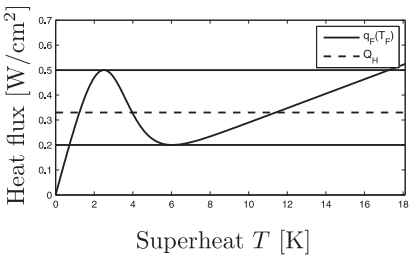

Figure 5.8: Nonlinear heat-flux function $q_F(T_F)$ according to the boiling curve of aluminum vs. FC-72, see [4]. The dashed line represents the nominal heat supply Q_H.

Heater height: $H = 3.5\text{mm}$

Controller and observer parameters are again according to (5.25). In Fig.5.9(a) the simulated evolution of the interface temperature ($T_F(x,t) := T(x,H,t)$) is shown (progression in time is again indicated by darker shades of grey of the intermediate profiles). Similar as for the IGBT cooling example an essentially heterogeneous initial state is regulated to the final homogeneous state. This means that disturbances that arise during operation can be suppressed effectively, resulting in constant and uniform temperatures in favour of a uniform temperature distribution throughout the battery pack. As can be seen, the region of attraction is quite large in this case as well. The too low initial temperature is increased by the controller by removing less heat from the battery. As a result, the battery warms itself until it reaches the desired temperature. The initial temperature fluctuations in x-direction are rapidly smoothed out, resulting in a homogeneous temperature distribution in the cell. This means temperature fluctuations can be smoothed very effectively by the thermal management scheme.

The temperature as function of time in the validation points is given in Fig. 5.9(b). Again the observer state quite rapidly converges to the system state. Due to the initial error, the

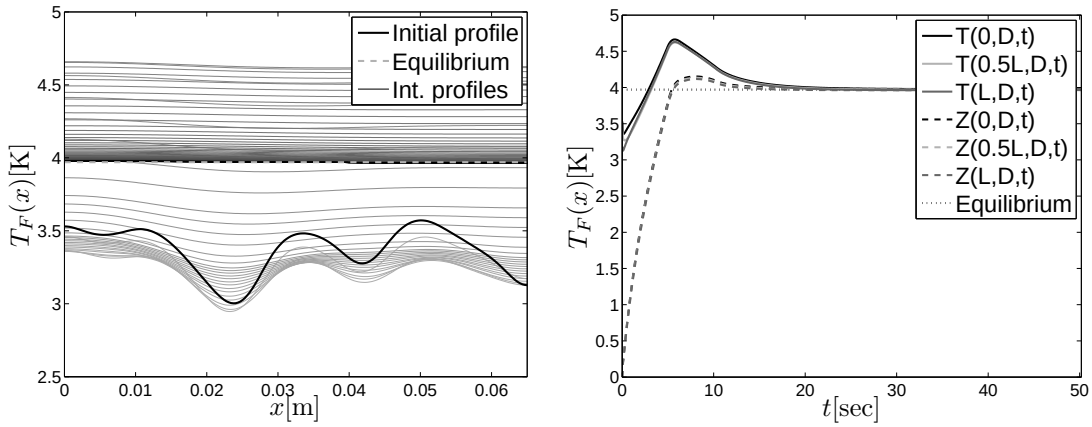

(a) Evolution of T_F as function of x

(b) Evolution of T_F as function of t

Figure 5.9: The evolution of the interface temperature $T_F(x,t)$ is shown for the battery-cooling case study, $H = 3.5$mm. The thin grey lines (in panel a) are intermediate profiles, progression in time is indicated by darker shades of grey. In panel b the evolution in the points $x = 0$, $x = \frac{1}{2}L$ and $x = L$ is shown for the system (solid line) and the observer (dashed line).

system overshoots its equilibrium value, however. After the observer state has reached the equilibrium the system state is regulated towards the equilibrium as well.

Finally, the input used to stabilise the equilibrium is given as function of time in Fig. 5.10. Initially, the input is taken maximal, then minimal and subsequently it smoothly converges to zero as the system state converges on the equilibrium.

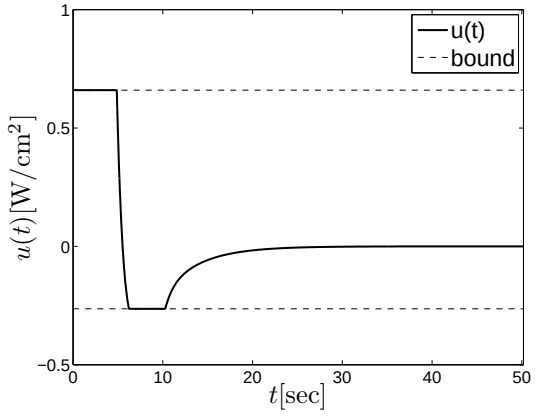

Figure 5.10: The input as function of time is shown for the battery-cooling case study, $H = 3.5$mm. The bounds of the input are given by the dashed lines.

Heater height: $H = 1.75$**mm**

If the heater is $H = 1.75$mm of height, the transition to film boiling can not be stabilised, since the interface temperature converges to a non-uniform state (partial vapour blanket).

This represents a temperature non-uniformity in the battery cell, which is undesired. The controller parameters are taken according to (5.25). In Fig. 5.11(a) the evolution of the fluid-heater interface temperature is shown. Although the initial condition is taken quite close to the equilibrium, the small perturbations are amplified by the boiling process resulting in a non-uniform temperature distribution. As before, this can not be remedied by taking different controller parameters. Furthermore, the distributions represent local hot regions and local cold regions. Although the temperature non-uniformity does not exceed approximately 3K for this individual cell, it can accumulate to quite large differences in an entire battery pack.

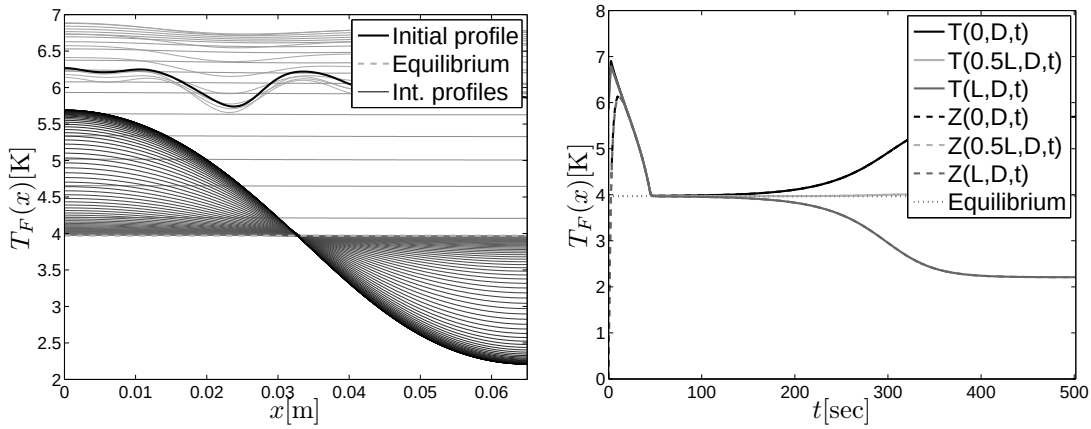

(a) Evolution of T_F as function of x

(b) Evolution of T_F as function of t

Figure 5.11: The evolution of the interface temperature $T_F(x,t)$ is shown for the battery-cooling case study, $H = 1.75$mm. The thin grey lines (in panel a) are intermediate profiles, progression in time is indicated by darker shades of grey. In panel b the evolution in the points $x = 0$, $x = \frac{1}{2}L$ and $x = L$ is shown for the system (solid line) and the observer (dashed line).

Fig. 5.11(b) depicts the evolution of the system and observer state in the validation points. The figure shows that the non-uniformity is not the result of poor observer performance as the observer state converges to the system state quite rapidly. Furthermore, it can be seen that initially the controller keeps the system at its equilibrium, but then small fluctuations in x-direction are amplified and in the system converges to the non-uniform state.

In Fig. 5.12 the input as function of time is given. Again the input settles at a nonzero value due to the fact that the system has not converged on the equilibrium.

5.4.3 Conclusion

In this study, a 2D nonlinear heat-transfer model for a boiling-based cooling device for cooling of Insulated Gate Bipolar Transistors (IGBTs) and battery thermal management in Electric Vehicles is considered. The model involves only the temperature distribution within the heater, i.e. a thermally conducting element between the to-be-cooled device and the boiling liquid. The heat exchange with the boiling medium is modelled via a nonlinear boundary condition imposed at the fluid-heater interface. In order to apply boiling at its fullest efficiency, unstable modes in the system must be stabilised.

To this end, a controller is introduced that regulates the pressure in the boiling system as a function of the heater temperature. by increasing (decreasing) the pressure, boiling can

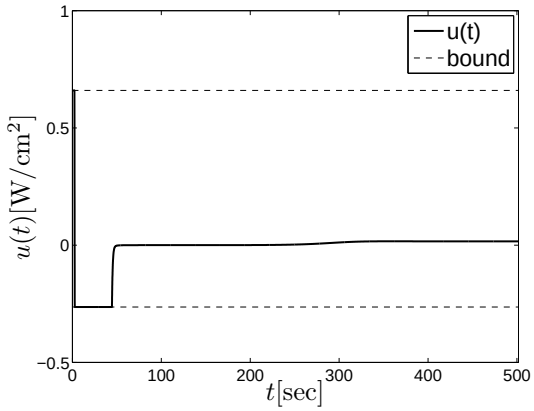

Figure 5.12: The input as function of time is shown for the battery-cooling case study, $H = 1.75$mm. The bounds of the input are given by the dashed lines.

be suppressed (stimulated) and as a result, more (less) heat can be extracted from the heater by the boiling liquid. In this way the boiling system can be kept in the efficient nucleate boiling regime. The entire temperature profile within the heater is estimated by an observer using only two measurements, both on top of the heater. Previous analyses have shown that controllers based on the dominant modes of the temperature profile within the heater are effective, see [17]. For this reason, the controller developed for this system is based on these modes as well.

The control strategy filters the Chebyshev-Fourier-cosine modes of the temperature profile of the heater. These modes are intimately related to the eigenmodes of the system. Therefore, the dynamics are mainly prescribed by the dominant modes, that is, the lower order Chebyshev-Fourier-cosine modes. The feedback law thus enables control of exactly those relevant lower order modes.

The observer is a copy of the nonlinear pool boiling model with an extra term in the boundary condition for the fluid heater interface, i.e. the top of the heater, by which convergence of the observer state on the system state is to be accomplished. This extra term accounts for the error between observer and system state on the fluid-heater interface.

Local asymptotic stability can be established via the linearised system and observer. Satisfactory closed-loop behaviour is obtained by fine-tuning of the control parameters using a characteristic equation which is derived using the method of separation of variables.

The performance of the control law for stabilisation of the nonlinear system is investigated in order to establish its value for practical purposes. Relevant issues are the asymptotic stability and evolution of the nonlinear closed-loop system. Simulations are performed for two case studies: (i) IGBT cooling and (ii) battery thermal management. It turns out that the closed-loop behaviour of the system is dependent on the system parameters such as height of the heater.

The first case study reveals convergence of the evolution of the nonlinear system on the unstable steady state for a wide range of initial states in case $H = 20$mm. These findings imply that the control loop indeed is capable of robustly stabilising the pool-boiling system for these parameters. For a thinner heater, $H = 8$mm, however, convergence of the nonlinear system on an essentially non-uniform state is observed. The final state has a region with temperatures

corresponding to nucleate boiling ('cold spots') and has a region corresponding to film boiling ('hot spots'). This results in local 'hot-spots' on the IGBT and is highly undesired since it can lead to failure of the device. In some cases, this phenomenon can be remedied by varying the nominal pressure in the boiling chamber. However, for these heater properties the only measure is stabilisation of the nucleate boiling equilibrium. A safety margin needs to be taken into account for this measure, though, this affects the cooling efficiency negatively.

If boiling is applied to the individual cells in a battery pack, the net evaporation/condensation of the boiling liquid plays a significant role as the volume of the pool is much smaller due to the closely packed battery cells. Physical considerations suggest that this can in a first approximation be modelled by a rescaled boiling curve. Therefore, thermal management of these cells, in spite of their low heat generation, still is a challenge, since non-uniform temperatures and local 'hot spots' may still occur. The case study reveals that convergence to the unstable uniform transition boiling equilibrium can nonetheless be achieved for $H = 3.5$mm. For this case study, similar as for the IGBT-cooling case study, also convergence to a non-uniform state is observed for a thinner heater, i.e. $H = 1.75$mm. This is highly undesired in battery thermal management, as it leads to more rapid battery deterioration.

Nevertheless, both case studies show that the efficiency of boiling-based cooling schemes can be increased by dynamically varying the pressure inside the boiling chamber. This puts forth boiling heat transfer as a promising solution for thermal management issues in electric vehicles. During the design process heater material and dimensions must be chosen carefully, though.

6 Conclusions

In this study several Battery Electric Vehicles (BEVs) and Hybrid Electric Vehicles (HEVs) are examined. The main conclusion concerning BEVs on todays automotive market is that their battery can be cooled passively by air. For HEV battery packs cooling is a little bit more critical as their charge/discharge profiles are more aggressive and more power must be supplied. However, a single-phase liquid cooling scheme suffices in HEV applications.

On the other hand recovering the minimal amount of heat that can be recovered by a battery thermal management system can seriously increase the range per charge of the BEV. In city driving, average vehicle speeds are low, moreover, heat generation in IGBTs and batteries is high due to the high frequency of regenerative braking and rapid accelerating of the vehicle. As a result, recovering the waste heat of the IGBTs and (to less extend) the batteries and re-use it to heat the cabin of the vehicle increases the vehicle range significantly. For example, heating power requirements 3 – 4 kW can decrease the range of BEVs in city driving with more than 50%. Recovering the waste heat of electrical components and using it to heat the cabin thus can help to increase the range of BEVs. At higher speeds, e.g. highway driving, this effect tones down, yet is still significant, as is discussed in Chapter 3.

However, if BEV battery packs are not thermally managed, this can result in reduced range and lifetime of the batteries and thus the vehicle. In Chapter 4 it is recapitulated that operation at increased temperatures of only 10 – 20 K can seriously reduce battery lifetime by several hundreds of cycles. Operation of Sony 18650 Li-ion cells at 50°C, for example, resulted in 50% capacity loss after only 600 cycles and even 70% capacity loss at 55° after only 500 cycles, which is, compared to the 31% capacity loss after 800 cycles at 25°C, a massive increase of degradation at these elevated temperatures. With respect to battery lifetime/deterioration, it thus is necessary to implement better thermal management schemes in EVs.

Furthermore, a thermal management system can increase the degree of temperature uniformity in the pack, which can increase battery lifetime as well. Since if the cells and modules in the pack are at different temperatures, each module will be charged/discharged slightly differently during each cycle. After several cycles, modules in the pack will become unbalanced, degrading the pack's performance. Hence, especially in consideration of cycle life of the battery pack a thermal management/homogenisation scheme is indispensable as is discussed in Chapter 4.

Moreover, although single phase liquid cooling in HEVs and air cooling in BEVs seems to be able to do the trick in current EVs, development of battery technology continues, introducing the need for more advanced cooling schemes. The single-phase cooling loops in HEVs require bulky electrical pumps to circulate the coolant, enhanced cooling methods based on natural convection might be interesting, so as to decrease the energy requirements and overall weight of the cooling scheme.

Not only the battery pack is a source of thermal issues in EVs, cooling of chips, or Insulated Gate Bipolar Transistors (IGBTs), is a challenge as well. To overcome overheating of these high power switching devices research on micro-channel flow boiling is conducted. As micro-channel flow boiling and pool boiling have essential similarities, the research of pool-boiling phenomena fits in this respect as well.

The thermal issues discussed above can be solved by application of boiling heat transfer. The key advantages of a boiling-based cooling schemes in EVs are (i) large cooling capacities, (ii) the reduction of weight compared to the weight of a single-phase cooling loop, (iii) temperature uniformity of the battery in favour of battery lifespan and (iv) waste heat recovery for cabin heating. To prevent the high power switching devices or IGBTs from overheating, a large heat flux per square cm is required. This can be obtained by applying boiling heat transfer to the chips. As the energy density per unit mass of the coolant is much larger than that of a single-phase cooling loop, the mass of the required coolant in the cooling design is much lower. Since boiling heat transfer occurs at a constant temperature irrespective of the heat flux, thermal management by boiling heat transfer allows for optimal temperature homogenisation of the battery. As boiling heat transfer allows for quick and intensive cooling, the removed heat can be released easily and effectively by condensation to any desired surface, for example for cabin heating.

Hence, the project where pool-boiling phenomena are investigated by a pool-boiling model seems to fit well in the "Range Extender Innovations (REI)" project of the High Tech Automotive Systems (HTAS) programme.

Acknowledgements

This research is funded by the HTAS-REI (Range Extender Innovations) project.

Bibliography

[1] S. Al Hallaj and J. Selman, *A novel thermal management system for electric vehicle batteries using phase-change material*, Journal of the electrochemical society, 147 (2000), pp. 3231 – 3236.

[2] A. Alrashdan, A. T. Mayyas, and S. Al-Hallaj, *Thermo-mechanical behaviors of the expanded graphite-phase change material matrix used for thermal management of li-ion battery packs*, Journal of Materials Processing Technology, 210 (2010), pp. 174–179.

[3] H. Auracher and W. Marquardt, *Experimental studies of boiling mechanisms in all boiling regimes under steady-state and transient conditions*, International Journal of Thermal Sciences, 41 (2002), pp. 586–598.

[4] H. Auracher and W. Marquardt, *Heat transfer characteristics and mechanisms along entire boiling curves under steady-state and transient conditions*, International Journal of Heat and Fluid Flow, 25 (2004), pp. 223–242.

[5] S. Barnes, F. Fleming, W. Longardner, and A. Rafalovich, *Thermal management for HEV valve-regulated lead-acid batteries*, in Proceedings of the 12th annual international electric vehicle symposium, December 1994, pp. 27 – 37.

[6] K. Bennion and M. Thornton, *Integrated vehicle thermal management for advanced vehicle propulsion technologies*, in SAE world congress, Detroit, Michigan, USA, April 13 – 15, 2010.

[7] G. Berdichevsky, K. Kelty, J. Straubel, and E. Toomre, *The tesla roadster battery system*. Tesla Motors, August 16, 2006.

[8] I. Besselink, P. van Oorschot, and H. Nijmeijer, *Design of an efficient, low weight battery electric vehicle based on a vw lupo 3l*, in The 25th world battery, hybrid and fuel cell electric vehicle symposium and exhibition (EVS-25), Shenzhen, China, November 5 – 9, 2010.

[9] J. Blum, W. Marquardt, and H. Auracher, *Stability of boiling systems*, International Journal of Heat and Mass Transfer, 39 (1996), pp. 3021–3033.

[10] C. Canuto, M. Hussaini, A. Quarteroni, and T. Zang, *Spectral Methods in Fluid Dynamics*, Springer, New York, third ed., 1988.

[11] Y. Chen and J. Evans, *Heat transfer phenomena in lithium/polymer-electrolyte batteries for electric vehicle application*, J. Electrochem. Soc., 140 (1993), pp. 1833 – 1838.

[12] R. Chu, R. Simons, M. Ellsworth, R. Schmidt, and V. Cozzolino, *Review of cooling technologies for computer products*, IEEE Transactions on Device and Materials Reliability, 4 (2004), pp. 568–585.

[13] V. Dhir, *Boiling heat transfer*, Annu. Rev. Fluid Mech., 30 (1998), pp. 365–401.

[14] C. DUSTMANN, *Advances in zebra batteries*, Journal of Power Sources, 127 (2004), pp. 85 – 92.

[15] S. GARIMELLA AND T. HARIRCHIAN, *Boiling heat transfer and flow regimes in microchannels – a comprehensive understanding*, in 15th International Workshop on Thermal Investigation of ICs and Systems (Therminic) 2009, Leuven, Belgium, October 7 – 9, 2009, pp. 101– 112.

[16] R. VAN GILS, M. SPEETJENS, AND H. NIJMEIJER, *Feedback stabilisation of a one-dimensional nonlinear pool-boiling system*, International Journal of Heat and Mass Transfer, 53 (2010), pp. 2393–2403.

[17] R. VAN GILS, M. SPEETJENS, AND H. NIJMEIJER, *Feedback stabilisation of two-dimensional non-uniform pool-boiling states*, in Advanced Computational Methods and Experiments in Heat Transfer XI, B. Sundén, U. Mander, and C. Brebbia, eds., Tallin, Estonia, July 14 – 16, 2010, WIT Press, pp. 215 – 226.

[18] R. VAN GILS, M. SPEETJENS, AND H. NIJMEIJER, *Feedback stabilization of transition boiling states*, in Proceedings of the 12th IEEE Intersociety Conference on Thermal and Thermomechanical Phenomena in Electric Systems (ITherm 2010), no. 044, Bally's, Las Vegas, Nevada, USA, June 2 – 5, 2010.

[19] R. VAN GILS, M. SPEETJENS, AND H. NIJMEIJER, *Boiling heat transfer in battery electric vehicles*, in EEVC 2011, Brussels, Belgium, October 26 – 28, 2011.

[20] R. VAN GILS, M. SPEETJENS, AND H. NIJMEIJER, *Feedback stabilisation of a two-dimensional pool-boiling system by modal control*, Int. J. of Thermal Sciences, (2012). submitted for publication.

[21] L. GUZZELLA AND A. SCIARRETTA, *Vehicle Propulsion Systems*, Springer, Berlin, second ed., 2007.

[22] E. HANSEN, L. WILHELM, N. KARDITSAS, I. MENJAK, D. CORRIGAN, S. DHAR, AND S. OVSHINSKY, *Full system nickel-metal hyrdide battery packs for hybrid electric vehicle applications*, in Battery conference on applications and advances, 2002. The seventeenth annual, Long Beach, CA , USA, 15 – 18 Jan. 2002, pp. 253 – 260.

[23] T. HECKENBERG, *Li-ion battery cooling: more than just another cooling task*, internal report, BEHR, 2009.

[24] R. HOHL, J. BLUM, M. BUCHHOLZ, T. LÜTTICH, H. AURACHER, AND W. MARQUARDT, *Model-based experimental analysis of pool boiling heat transfer with controlled wall temperature transients*, International Journal of Heat and Mass Transfer, 44 (2001), pp. 2225–2238.

[25] J. HSU, R. STAUNTON, AND M. STARKE, *Barriers to the application of high-temperature coolants in hybrid electric vehicles*, Technical report ORNL/TM-2006/514, Oak Ridge National Laboratory, 2006.

[26] I. HUSAIN, *Electric and hybrid vehicles, design fundamentals*, CRC press, first ed., 2003.

[27] S. G. KANDLIKAR, *Critical heat flux in subcooled fow boiling – an assesment of current understanding and future directions for research*, Multiphase Sci Technol., 13 (2001), pp. 207 – 232.

[28] S. G. KANDLIKAR, *Heat transfer mechanisms during flow boiling in microchannels*, ASME J. Heat Transfer, 126 (2004), pp. 8 – 16.

[29] S. G. KANDLIKAR, *Similarities and differences between flow boiling in microchannels and pool boiling*, in Proceedings of the second micro and nano flows conference, West London, 2009.

[30] P. A. KEW AND K. CORNWELL, *Correlations for the prediction of boiling heat transfer in small-diameter channels*, Applied Thermal Engineering, 17 (1997), pp. 705–715.

[31] V. KHANNA, *The insulated gate bipolar transistor: IGBT theory and design*, Wiley, first ed., 2003.

[32] S. KHATEEB, M. FARID, J. SELMAN, AND S. AL-HALLAJ, *Design and simulation of a lithium-ion battery with a phase change material thermal management system for an electric scooter*, Journal of Power Sources, 128 (2003), pp. 292 – 307.

[33] S. A. KHATEEB, S. AMIRUDDIN, M. FARID, J. R. SELMAN, AND S. AL-HALLAJ, *Thermal management of li-ion battery with phase change material for electric scooters: experimental validation*, Journal of Power Sources, 142 (2005), pp. 345–353.

[34] E. KREYSZIG, *Advanced Engineering Mathematics*, Wiley, New York, eighth ed., 1999.

[35] P. KRONER, *Thermal comfort in the vehicle. new vehicle designs require new a/c solutions*, internal report, BEHR, 2009.

[36] J. LARMINIE AND J. LOWRY, *Electric vehicle technology explained*, Wiley, first ed., 2003.

[37] B. MCKINNEY, G. WIERSCHEM, AND E. NROTEK, *Thermal management of lead-acid batteries for electric vehicles*, in Batteries for electric vechicle-research development and testing conference, Detroit, Michigan, USA, February 28, 2003.

[38] A. MILLS AND S. AL-HALLAJ, *Simulation of passive thermal management system for lithium-ion battery packs*, Journal of Power Sources, 141 (2005), pp. 307–315.

[39] I. MUDAWAR, *Assessment of high-heat-flux thermal management schemes*, IEEE Transactions on Components and Packaging Technologies, 24 (2001), pp. 122–141.

[40] P. VAN OORSCHOT, *Battery test: Thundersky lfp90aha*, tech. report, Eindhoven University of Technology, Department of Mechanical Engineering, Dynamics and Control Group, 2010.

[41] P. VAN OORSCHOT, I. J. M. BESSELINK, AND H. NIJMIJER, *Realization of an ev research platform and its range estimation*, -, (2011), pp. xx – xx. (In preparation).

[42] P. VAN OORSCHOT AND R. VOS, *Electric vehicle test: Vw golf variant ece*, Tech. Report DC 2010.036, Eindhoven University of Technology, Department of Mechanical Engineering, Dynamics and Control Group, 2010.

[43] H. VAN OUWERKERK, *Burnout in pool boiling the stability of boiling mechanisms*, International Journal of Heat and Mass Transfer, 15 (1972), pp. 25–34.

[44] A. PAL, Y. JOSHI, M. BEITELMAL, C. PATEL, AND T. WENGER, *Design and performance evaluation of a compact thermosyphon*, in Thermes, Sante Fe, USA, jan 13-16 2002, pp. 251 –260.

[45] A. PESARAN, *Battery thermal management in EV's and HEV's: Issues and solutions*, in Proceedings of the Advanced Automotive Battery Conference, Las Vegas, Nevada, USA, February 6 – 8, 2001.

[46] A. PESARAN, *Current and future needs in electric drive vehicle batteries*, in Proceedings of the 14th international heat transfer conference, IHTC14, Washington DC, USA, August 8 – 13, 2010.

[47] A. PESARAN, T. MARKEL, H. TATARIA, AND D. HOWELL, *Battery requirements for plug-in hybrid electric vehicles – analysis and rationale*, in 23rd International electric vehicle symposium (EVS-23), Anaheim, California, USA, December 2 – 5, 2007.

[48] A. PESARAN, A. VLAHINOS, AND S. BURCH, *Thermal performance of EV and HEV battery modules and packs*, in Proceedings of the 14th international electric vehicle symposium, Orlando, Florida, December 15 – 17, 1997.

[49] A. PESARAN, A. VLAHINOS, AND T. STUART, *Cooling and preheating of batteries in hybrid electric vehicles*, in 6th ASMR-JSME Thermal Engineering Conference, Hawaii, USA, March 16 – 20, 2003.

[50] P. RAMADASS, B. HARAN, R. WHITE, AND B. POPOV, *Capacity fade of sony 18650 cells cycled at elevated temperatures: Part ii. capacity fade analysis*, Journal of Power Sources, 112 (2002), pp. 614–620.

[51] M. SPEETJENS, *Steady-state behavior of a three-dimensional pool-boiling system*, J. Electron. Packag., 130 (2008), pp. 041102–7.

[52] M. SPEETJENS, A. REUSKEN, S. MAIER-PAAPE, AND W. MARQUARDT, *Stability analysis of two-dimensional pool-boiling systems*, SIAM Journal of Applied Dynamical Systems, 7 (2008), pp. 933–961.

[53] M. SPEETJENS, A. REUSKEN, AND W. MARQUARDT, *Steady-state solutions in a nonlinear pool boiling model*, Communications in Nonlinear Science and Numerical Simulation, 13 (2006), pp. 1475–1494.

[54] M. SPEETJENS, A. REUSKEN, AND W. MARQUARDT, *Steady-state solutions in a three-dimensional nonlinear pool-boiling heat-transfer model*, Communications in Nonlinear Science and Numerical Simulation, 13 (2006), pp. 1518–1537.

[55] J. R. THOME, *Boiling in microchannels: a review of experiment and theory*, International Journal of Heat and Fluid Flow, 25 (2004), pp. 128–139.

[56] WEBSITE, *http://thinkev.com/*, visited in August 2010. Official website Think City Electric Vehicle.

[57] WEBSITE, *http://www.chevrolet.com/pages/open/default/future/volt.do*, visited in August 2010. Official Chevrolet Volt website.

[58] WEBSITE, *http://www.ener1.com/?q=content/enerdel-main*, visited in August 2010. Official website of Enerdel.

[59] WEBSITE, *http://www.greencarcongress.com/2009/09/garimella-20090923.html*, visited in August 2010. Green car congress website.

[60] WEBSITE, *http://www.nissanusa.com/leaf-electric-car*, visited in August 2010. Official U.S. Nissan Leaf website.

[61] M.-S. WU, K. H. LIU, Y.-Y. WANG, AND C.-C. WAN, *Heat dissipation design for lithium-ion batteries*, Journal of Power Sources, 109 (2002), pp. 160–166.

[62] M. ZOLOT, K. KELLY, M. KEYSER, M. MIHALIC, AND A. PESARAN, *Thermal evaluation of the honda insight battery pack*, in the 36th intersociety energy conversion engineering conference (IECEC'01), Savannah, Georgia, USA, July 29 - August 2, 2001.

[63] M. ZOLOT, A. PESARAN, AND M. MIHALIC, *Thermal evaluation of toyota prius battery pack*. National Renewable Energy Laboratory, 2002.

A Paper EEVC

In the following the paper that has been published in the proceedings of the European Electric Vehicle Conference (EEVC), [19], is given.

EEVC
Brussels, Belgium, October 26-28, 2011

Boiling Heat Transfer in Battery Electric Vehicles

Rob van Gils[1,*], Michel Speetjens[2], Henk Nijmeijer[1]
[1]*Eindhoven University of Technology, Department of Mechanical Engineering, Dynamics and Control group*
[2]*Eindhoven University of Technology, Department of Mechanical Engineering, Energy Technology group*
[*]*Corresponding author, P.O Box 513, WH -1.144, 5600 MB, Eindhoven,* r.w.v.gils@tue.nl

Abstract

In this paper the feedback stabilisation of a boiling-based cooling scheme is discussed. Application of such cooling schemes in practical setups is greatly limited by the formation of a thermally insulating vapour film on the to-be-cooled device, called burn-out. In this study a first step is made, to check the viability of such cooling systems, already used in high performance electronics, applied to Electric Vehicles (EVs). It can be used for instance for the cooling of high heat flux transistors and for the thermal homogenisation of battery packs. Thereto, the unstable transition to burn-out is stabilised by controlling the pressure inside the boiling chamber, with which boiling (and thus creation of the thermally insulating vapour film) can be stimulated or suppressed. The feedback law used to do this is based on the dominant modes of the temperature field of the thermally conducting element, i.e. the heater, between the device and the boiling liquid. As not all states used in this feedback law can be measured, an observer or "state-estimator" must be implemented in the control strategy. The observer is a copy of the nonlinear boiling model with an additional term to assure convergence of observer to system state. Simulations are performed to demonstrate controller efficiency on the nonlinear cooling device. This puts forth the boiling-based cooling scheme as viable for application in EVs, enabling increased cooling and thermal-homogenisation capacities compared to conventional thermal management methods. The next step should be experiments to proof the principle on battery cells/packs and high heat flux transistors.

Keywords: BEV, Battery thermal management, Cooling, boiling, numerical simulation

1 Introduction

During fast acceleration and regenerative braking in electric vehicles (EVs), the high-power switching devices, that switch large amounts of power from the battery pack to the electrical coils of the electric motors, produce significant amounts of heat. To prevent these so-called insulated gate bipolar transistors (IGBTs) from overheating during these actions, boiling heat transfer is the pre-eminent choice as the cooling mechanism. Boiling heat transfer namely allows for *quick* and *intensive* cooling. Moreover, the evaporated fluid can be easily transported throughout the vehicle, and the removed heat can be released to any desired surface via condensation. In this way, the removed heat can be used, for instance to heat the vehicle cabin, decreasing the auxiliary power requirements. In addition, due to natural convection, no (large) pumps are required to circulate the fluids. Thus thermal management based on boiling heat transfer can significantly increase the range per charge of Battery Electric Vehicles (BEVs) [1], which is currently considered to be their main drawback, [2].
Boiling heat transfer can also be applied as battery thermal management system. Operation at elevated temperatures can seriously accelerate battery deterioration, see [3]. While operation at lowered temperatures can seriously decrease the efficiency of the battery, see [1]. Furthermore, due to the passive working principle, boiling heat transfer can also be applied when the car is turned off, e.g. when the car is parked in the sun. Another important parameter with respect

to the battery lifespan is the temperature uniformity of the battery, see [4]. Hence, especially in consideration of cycle life of the battery pack, a thermal management/homogenisation scheme is indispensable. Boiling heat transfer allows for thermal homogenisation very effectively as it, irrespective of heat fluxes, happens at fixed temperatures for given pressure, see [5].
However, full exploitation of boiling heat transfer for thermal management is severely limited by the risk of 'burn-out', i.e. the sudden formation of a vapour blanket on the heating device that leads to a catastrophic temperature jump and, in consequence, an abrupt collapse of the cooling and homogenisation capacity [6]. Insight into the complex boiling dynamics underlying "burn-out" and into ways to actively control it, is imperative to overcome this hazard.
Pool boiling may serve as physical representation for cooling applications based on boiling heat transfer. Such systems consist of a heater submerged in a pool of boiling liquid. This is depicted in Fig.1, the to-be-cooled device supplies heat to the bottom wall of the heater, which corresponds with a thermally conducting element between the actual heat source (e.g. a battery cell) and the coolant at the top wall of the heater. The boiling liquid extracts heat from the heater and releases thermal energy through the escaping vapour. The vapour turns into liquid again in a condenser, releasing the heat taken up, and flows back towards the boiling liquid.

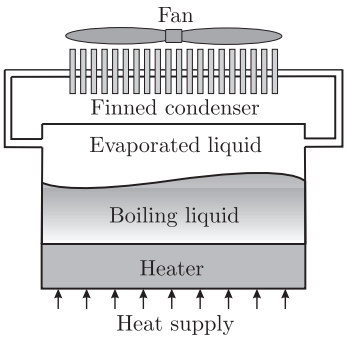

Figure 1: Schematic representation of a pool-boiling system.

Pool boiling is characterised by three boiling regimes through which the system progresses with increasing temperature on the fluid-heater interface: nucleate, transition and film boiling [7]. Nucleate boiling is, as opposed to film boiling, an efficient and safe mode of heat transfer and is the desired boiling mode in most practical applications. Nucleate boiling transits into film boiling upon exceeding the so-called critical heat flux (CHF) through the intermediate state of transition boiling. This transition is highly unstable and causes a sharp *increase* in temperature and *decrease* in heat flux. This is the result of the sudden formation of a thermally-insulating vapour film on the fluid-heater interface [6]. Transition, thus, leads to the collapse of the cooling and homogenisation capacity and must be avoided in practical thermal management systems [7].

Hence, utilising boiling heat transfer for cooling entails a trade-off between efficiency (close proximity to CHF) and safe operation (certain distance from CHF). Current cooling schemes require a relatively large safety margin due to two key limitations: (i) high uncertainty in predicting CHF and system dynamics; (ii) the inability to actively respond to fluctuating cooling demands due to the passive working principle [8]. Robust control strategies that safely facilitate boiling heat transfer close to CHF under dynamic operating conditions offer a promising solution, yet their realisation poses a formidable challenge.

As a result, to date theoretical studies for pool boiling applications are scarce. There is a large data-base on boiling experiments, though. However, the CHF depends, next to the fluid-heater combination, on numerous other variables, such as surface roughness and system pressure. Consequently, experimental results can only be used in a very limited range of boiling applications, see e.g. [6, 9]. Theoretical pool boiling investigations are presented in [10] where a one-dimensional (1D) system is stabilised by way of linearisation of the boiling curve around the homogeneous transition state. In [11] a more realistic pool boiling model is formulated which leans on the phenomenological connection between the local boiling mode and the interface temperature and describes the system dynamics entirely in terms of the temperature distribution within the heater. In [12, 13] the two-dimensional (2D) nonlinear heater-only model is analysed for equilibria and stability properties. Successful stabilisation of the one-dimensional (1D) simplification of this model has been achieved in [14] by regulation of the heat supply via a linear state feedback based on the internal temperature profile. Most recent investigations of stabilisation of unstable steady states of the original 2D model are presented in [15, 16].

Key to the proposed control strategy is the expression of the heater's temperature profile by Chebyshev and Fourier polynomials, which are intimately related to the physical eigenmodes of the 2D system. The smoothness of the temperature field within the heater ensures exponential convergence of the Chebyshev-Fourier spectrum and, consequently, accurate representation of its eigenmodes by lower-order Chebyshev and Fourier polynomials. This has the important implication that the system dynamics can be regulated on the basis of a few lower-order Fourier-Chebyshev modes of the temperature field.

This study aims to test this 2D modal control law for the purpose of thermal management in EVs by way of a performance analysis in an idealised system as first step towards realisation of a practical setup. Thereto, the dynamical behaviour of the system introduced in [16] is considered for realistic values of the physical parameters. The control law represents the dynamical variation of the system pressure, with which the onset of film boiling is to be prevented. The simulations represent two thermal issues in EVs, being (i) IGBT-cooling and (ii) thermal homogenisation of the battery pack. These simulations are a first step towards realisation of a practical setup.

For the IGBT-cooling case study, a 80×80mm IGBT that produces 15W/cm^2 of heat is considered [17]. For the second case study the thermal homogenisation of a small battery cell, like for example used in the Tesla Roadster, 65mm of length, is considered. The cell is assumed to produce 0.33W/cm^2 of heat [18]. In both cases the heater is assumed to be made out of aluminum with dimensions $L \times H$. Its length is equal to that of the to-be-conditioned device: $L = 80$mm for the IGBT and $L = 65$mm for the battery cell. Its height is to be specified hereafter. The fluorinated liquid FC-72 (C_6F_{14}, 3M company) with a boiling point of $T_{\text{sat}} = 56°$C at atmospheric pressure, is considered to be the coolant.

2 Model description

The model to represent the thermal management scheme is based upon the two-dimensional (2D) heater-only model first presented in [12]. In this model, the boiling fluid is solely modelled by the boundary condition on top of the heater. This can be done because of a phenomenological connection between the boiling mode and the interface temperature, cf. [12]. In the following, this model, its equilibria and the linearisation around them are discussed.

2.1 Heater-only model

In the heater-only model, the heat transfer in the 2D rectangular heater $\mathcal{H} = [0, L] \times [0, H]$ is considered – see Fig.2. The boundary segments of the heater are given by (i) adiabatic sidewalls for $x = 0$ and $x = L$, (ii) a constant heat supply extended with the system input by which unstable states must be stabilised at $y = 0$, and (iii) the nonlinear heat extraction by the boiling process on top of the heater at $y = H$.

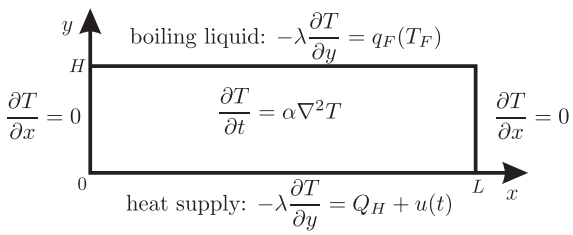

Figure 2: Heater configuration of the pool-boiling model.

The model describes the heat transfer in terms of the superheat $T(x, y, t)$, i.e. the temperature relative to the boiling point of the coolant. The superheat $T(x, y, t)$ within the heater is given by the heat equation

$$\frac{\partial T}{\partial t}(x, y, t) = \alpha\nabla^2 T(x, y, t), \tag{1}$$

with the boundary conditions

$$\left.\frac{\partial T}{\partial x}\right|_{x=0,L} = 0, \tag{2}$$

$$\left.\frac{\partial T}{\partial y}\right|_{y=0} = -\frac{1}{\lambda}(Q_H + u(t)), \tag{3}$$

$$\left.\frac{\partial T}{\partial y}\right|_{y=H} = -\frac{1}{\lambda}q_F(T_F), \tag{4}$$

with $\lambda = 237$Wm^{-1}K^{-1} the thermal conductivity of the aluminum heater, L its length as defined in the Introduction, H its height, $T_F := T(x, H, t)$ the fluid-heater interface temperature, $\alpha = 8.42 \cdot 10^{-5}$m^2/s the thermal diffusivity of the heater, $q_F(T_F)$ the nonlinear heat flux relation given in Fig.3, $u(t)$ the system input and Q_H the nominal heat generation by the to-be-cooled device as defined in the introduction.
Burn-out is to be avoided by variation of the system pressure. Decreasing (increasing) p stimulates (suppresses) evaporation and thus will lead to burn-out faster (less fast). Decreasing (increasing) the pressure will thus decrease (increase) the CHF, i.e. the local maximum of $q_F(T_F)$ in Fig. 3, CHF $\propto p$. Although reduction (elevation) of the pressure is accompanied by a temperature decrease (increase), the temperature distribution will remain uniform and heat flux per unit area will remain high. By regulating the pressure, the system thus can be kept in the efficient nucleate boiling regime. In the model, decreasing (increasing) the system pressure is modelled by increasing (decreasing) the heat supply $Q_H + u(t)$, which will lead to burn-out faster (less fast), $u(t) \propto \text{CHF}^{-1} \propto p^{-1}$. As a result, the heat flux function $q_F(T_F)$ can be kept constant over time and system modelling simple.

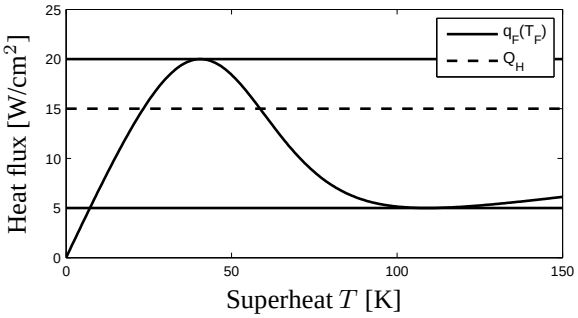

Figure 3: Nonlinear heat-flux function $q_F(T_F)$ according to the boiling curve of aluminum vs. FC-72, see [9]. The dashed line represents the nominal heat supply Q_H.

The nonlinear heat-flux function $q_F(T_F)$ describes the *local* heat exchange between the heater and the boiling fluid as function of the *local* fluid-heater interface temperature. On physical grounds, it is identified with the so-called

boiling curve, that is, the relation describing the *mean* heat exchange between heater and fluid along the *entire* fluid-heater interface (see [7]). This implies a functional relation $q_F(T_F)$ according to Fig.3. As can be seen, the function q_F comprises three distinct regimes, these correspond to one of the local boiling modes and associated boiling states: nucleate boiling (left of local maximum; fluid-rich state, efficient heat transfer), transition boiling (in between both extremes; transitional state) and film boiling (right of local minimum; vapour-rich state, inefficient heat transfer). If the heat supply exceeds CHF, the nucleate boiling regime ceases to exist, and passing through the transition boiling regime, the film boiling regime is entered. This is accompanied with a massive increase in temperature and thus is to be avoided in practical applications.

2.2 Equilibria of the model

An extensive exposition on the steady states of this model and their stability properties is furnished in [12, 13]. Below a concise recapitulation is provided.
Steady states $T_\infty(x, y)$ of (1-4) are found via application of the method of separation of variables, see [19]. This yields a (formal) solution given by

$$T_\infty(x,y) = \sum_{k=0}^{\infty} \widetilde{T}_k \frac{\cosh(\kappa_k y)}{\cosh(\kappa_k H)} \cos(\kappa_k x) + \frac{Q_H}{\lambda}(H-y), \tag{5}$$

with $\kappa_k = k\pi/L$ and coefficients $\widetilde{T}_k$ the spectrum of the Fourier cosine expansion of the temperature at the fluid-heater interface,

$$T_{F,\infty}(x) := T_\infty(x,H) = \sum_{k=0}^{\infty} \widetilde{T}_k \cos(\kappa_k x). \tag{6}$$

These coefficients are determined by the nonlinear Neumann condition at $y = H$, upon substitution of (5) leading to

$$\sum_{k=0}^{\infty} \widetilde{T}_k \kappa_k \tanh(\kappa_k H)\cos(\kappa_k x) - \frac{Q_H}{\lambda} = -\frac{1}{\lambda} q_F(T_{F,\infty}), \forall\ x \in [0,L]. \tag{7}$$

Equation (7) is the characteristic equation that determines the particular properties of the steady states of (1-4). If $\widetilde{T}_k = 0$ for $k > 0$, the equilibrium is constant in x-direction and (7) simplifies to $q_F(T_{F,\infty}) = Q_H$. As a result, $T_{F,\infty}$ coincides with the intersection(s) between the boiling curve (solid line in Fig.3) and the nominal heat-supply (dashed line in Fig.3). Here the left and right intersections correspond to stable nucleate and stable film boiling, respectively. The middle intersection corresponds to an unstable transition boiling equilibrium. These three equilibria are called the homogeneous equilibria as they are uniform in x-direction. All other equilibria are not uniform in x-direction and are called the heterogeneous equilibria. Heterogeneous solutions are characterised by local liquid-rich and local vapour-rich regions and thus belong to the transition boiling regime.
The principal objective here is the stabilisation of the unstable homogeneous transition equilibrium. Without stabilisation of this equilibrium, exceeding the CHF will inherently result in progression to the film boiling regime and burn-out of the to-be-cooled device. Stabilisation of this equilibrium, on the other hand, allows for increased heat flux rates and thus increases the efficiency of the cooling device. Because of the non-uniform temperature distribution of the heterogeneous equilibria, convergence towards these equilibria results in undesired non-uniform temperature distributions in the battery pack or IGBT and thus is to be avoided during operation.

2.3 Linearisation

Stabilisation of the homogeneous transition boiling equilibrium is investigated in terms of a linearisation of the pool boiling model around this equilibrium. To this end, small deviations $v(x, y, t)$ from the equilibrium $T_\infty(x, y)$ are considered, i.e. $T(x, y, t) = T_\infty(x, y) + v(x, y, t)$. Standard linearisation methods readily yield

$$\frac{\partial v}{\partial t}(x,y,t) = \alpha \nabla^2 v(x,y,t), \tag{8}$$

with the boundary conditions

$$\left.\frac{\partial v}{\partial x}\right|_{x=0,L} = 0, \tag{9}$$

$$\left.\frac{\partial v}{\partial y}\right|_{y=0} = -\frac{1}{\lambda}u(t), \tag{10}$$

$$\left.\frac{\partial v}{\partial y}\right|_{y=H} = -\frac{1}{\lambda}\gamma(x) v_F(x), \tag{11}$$

as linear counterpart of (1-4), where $v_F(x) := v(x, H)$ and

$$\gamma(x) = \left.\frac{\mathrm{d}q_F}{\mathrm{d}T_F}\right|_{T_F(x)=T_{F,\infty}(x)}. \tag{12}$$

3 Control strategy

In this section, the control strategy for stabilisation of the pool boiling system is discussed. Burn-out is to be avoided by variation of the system pressure p. In order to keep the heat flux function $q_F(T_F)$ constant over time and system modelling simple, this is modelled by uniform variation $u(t)$ of the heat supply, as discussed in the previous section.

3.1 Feedback law

The intended control strategy is a feedback law based on the deviation $v(x,y,t) = T(x,y,t) - T_\infty(x,y)$ between the heater superheat $T(x,y,t)$ and its desired distribution $T_\infty(x,y)$. Easily stated, if the temperature inside the heater is lower than the desired value, $u(t)$ is positive as a result of which boiling is stimulated and lower heat fluxes are generated between heater and boiling liquid. Consequently, the device is cooled less efficient and heats itself. When the temperature is too high, the input is negative and boiling is suppressed by increasing the pressure, as a result, higher heat fluxes are generated and more heat is extracted from the device, cooling it down in the process.
The input can be calculated by evaluating the heaters temperature in only one or two specific points, however, the aim here is to evaluate the entire temperature profile in the feedback law in favor of beneficial closed-loop behaviour, i.e. the behaviour of the system with the feedback law. The heater temperature $v(x,y,t)$ is multiplied with a feedback weightfunction $g(x,y)$ to be able to give more weight to specific regions within the heater, e.g. the fluid-heater interface. As system pressure is equal in the entire boiling chamber, the system input $u(t)$ must be uniform in x-direction. As a result, the term $v(x,y,t)g(x,y)$ must be integrated over the heater domain, resulting in the feedback law

$$u(t) = \int_0^H \int_0^L v(x,y,t)g(x,y)\mathrm{d}x\mathrm{d}y. \quad (13)$$

This means that the controller calculates whether the overall temperature in the heater is too high or too low and stimulates or suppresses the boiling process accordingly (specific regions can be excluded or be given more weight by appropriate choice of $g(x,y)$). With the feedback weight function the properties of the feedback law, and thus the closed-loop system, will be prescribed. Furthermore, the temperature inside the heater $v(x,y,t)$ is expressed in a form that is intimately related to its natural eigenmodes. This means that in x-direction, the eigenmodes of the Laplace operator are taken to represent the profile, i.e. by a Fourier-cosine expansion. In y-direction, the profile is expressed in the non-periodic variant of this expansion, i.e. the Chebyshev expansion. This control law is discussed in full detail in [15, 16], here only a concise recapitulation is given. The temperature profile in terms of the Chebyshev-Fourier spectrum is given by

$$v(x,y,t) = \sum_{k,n=0}^{\infty} \widetilde{v}_{nk}(t)\phi_n(\theta(y))\rho_k(x), \quad (14)$$

with $\widetilde{v}_{nk}$ the spectral coefficients of $v(x,y,t)$, $\phi_n(\theta) = \cos(n\arccos(\theta))$ is the n-th Chebyshev polynomial, $\rho_k(x) = \cos(\kappa_k x)$ the k-th Fourier cosine polynomial and $\theta = \frac{2}{H}y - 1$ is the computational domain in y-direction, cf. [20]. Note that here an infinite series is considered, meaning no approximation error is introduced in this step. Moreover, if a smooth temperature field in the heater is assumed, due to exponential convergence of the Chebyshev-Fourier-cosine spectral coefficients, the system dynamics are mainly prescribed by the 'lower order' modes, i.e. modes with low n *and* low k. As a result, the feedback law given by (13) only needs to be based on these 'lower' modes, as established in [14].
In order to filter these specific modes from the profile $v(x,y,t)$, the feedback weight function $g(x,y)$ is taken as

$$g(x,y) = \sum_{q,p=0}^{\infty} \widetilde{g}_{qp}\phi_q(\theta)w_C(\theta)\rho_p(x), \quad (15)$$

with $w_C(\theta) = (1-\theta^2)^{-\frac{1}{2}}$ the orthogonal weight function of the Chebyshev polynomials, cf. [20] and $\widetilde{g}_{qp}$ the spectral coefficients of the weight function. Due to the orthogonality property of the Chebyshev and Fourier polynomials, implementing (14) and (15) in (13) reduces the feedback law to

$$u(t) = \sum_{p,q=0}^{\infty} \widetilde{v}_{qp}(t)k_{qp}, \quad (16)$$

where $k_{qp} = \frac{\pi H}{8}c_q c_p \widetilde{g}_{qp}$ and the factor $c_i = 2$ for $i = 0$ and $c_i = 1$ for $i > 0$, see [20].
Note that this feedback law enables control of individual Chebyshev-Fourier-cosine modes by appropriate choice of k_{qp}. This so-called modal control scheme thus enables efficient control of exactly the relevant lower order modes. Meaning that this feedback law practically is a full-state feedback, which significantly outperforms standard P-control for this boiling application [14].
The elements k_{qp} must be determined such that desired/satisfactory closed-loop dynamics are obtained. This can be done by putting the so-called closed-loop poles of the linearised system at desired/satisfactory locations. To determine these closed-loop poles, a characteristic equation is derived analogously to the derivation of (7). The closed-loop poles of the system are given by the $\mu \in \mathbb{C}$ that satisfy

$$\begin{aligned}\sum_{k=0}^{\infty} A_k\rho_k(x)\left[\sqrt{\alpha_k}\tanh(\sqrt{\alpha_k}H) + \tfrac{1}{\lambda}\gamma(x)\right] \\ + \sum_{k=0}^{\infty} A_k F_k\left[\tfrac{1}{\lambda}\gamma(x) - \sqrt{\alpha_0}\right] = 0,\end{aligned} \quad (17)$$

for all $x \in [0, L]$, for nontrivial A_k (i.e. $A_k \neq 0$ for at least one k). The parameter α_k is given by

$$\alpha_k = \left(\frac{k\pi}{L}\right)^2 + \frac{\mu}{\alpha}. \quad (18)$$

and the closed-loop contribution F_k equals

$$F_k = \frac{\sum_{q=0}^{\infty} k_{qk}\xi_q^k}{\lambda\sqrt{\alpha_0} - \sum_{q=0}^{\infty} k_{q0}\zeta_q} \frac{e^{-\sqrt{\alpha_0}H}}{\cosh(\sqrt{\alpha_k}H)} \quad (19)$$

Furthermore, $(A_0 \cdots A_\infty)$ is the spectrum of the eigenmode of the closed-loop system that corresponds to the computed pole μ. The coefficients ξ^k and ζ are the spectral coefficients of the Chebyshev expansion of $\cosh\left(\sqrt{\alpha_k}\frac{H}{2}(\theta+1)\right)$ and $e^{-\sqrt{\alpha_0}\frac{H}{2}(\theta+1)}$, respectively. Approximations to the poles of the closed-loop system can be found via discretisation of (17). Derivation of this expression and determination of the poles is discussed in full detail in [15].
Using this equation, the closed-loop poles for a specific feedback law, i.e. with the elements k_{nk} given, can be determined. By varying one of the elements of the feedback law, e.g. k_{00}, the poles will move away from their original position. By plotting the path the dominant poles describe as function of the controller element, a pole-trajectory plot can be obtained. Using these plots, controllers that result in satisfying closed-loop behaviour are designed.

3.2 Observer design

It is important to note that, in practical applications, the state $T(x, y, t)$ (and thus $v(x, y, t)$) can only be measured at a finite number of points on the fluid-heater interface. Therefore, the control law discussed in the above necessitates an observer or "state-estimator", see [14]. This observer estimates the temperature profile out of available measurements of the heater temperature at the measurement points.
We assume that measurements are available at $x = 0$ and $x = L$ on the fluid-heater interface, i.e. at the top left corner and the top right corner of the heater. The error between the measurements and the output of the observer is used to approximate the error $E(x, y, t)$ between system state $T(x, y, t)$ and observer state $Z(x, y, t)$, on the entire fluid-heater interface, i.e. for $y = H$, meaning $E_F^{\text{ap}} \approx E(x, H, t) = T(x, H, t) - Z(x, H, t)$. The approximation E_F^{ap} is given by the Fourier expansion of the error in the measurement points $\widetilde{x}_r = r/R$ for $r = 0, ..., R$ and $R = 1$,

$$E_F^{\text{ap}}(x) = \sum_{r,p=0}^{R} \frac{\eta_r}{2R} E_F(\widetilde{x}_p)\rho_r(\widetilde{x}_p)\eta_p\rho_r(x), \quad (20)$$

where $\eta_i = 1$ for $i = 0 \vee K$ and $\eta_i = 2$ for $0 < i < K$. As observer we employ a copy of the nonlinear system with injection of E_F^{ap} on the boundary segment where the measurements are available, i.e. at the fluid-heater interface.

The observer thus is governed by

$$\frac{\partial Z}{\partial t}(x, y, t) = \alpha\nabla^2 Z(x, y, t), \quad (21)$$

with the boundary conditions

$$\left.\frac{\partial Z}{\partial x}\right|_{x=0,L} = 0, \quad (22)$$

$$\left.\frac{\partial Z}{\partial y}\right|_{y=0} = -\frac{1}{\lambda}(Q_H + u(t)), \quad (23)$$

$$\left.\frac{\partial Z}{\partial y}\right|_{y=H} = -\frac{1}{\lambda}q_F(Z_F) + qE_F^{ap}(x), \quad (24)$$

where q is the observer gain by which the observer error dynamics must be stabilised. Local stability of the observer error dynamics can be guaranteed via analysis according to (17) of the linearised observer error dynamics.

3.3 Controller-observer combination

The stability of the closed-loop system is only guaranteed in a small region around the to-be-stabilised equilibrium (local asymptotic stability) as it is based on the linearisation of the nonlinear system and observer. The so-called region of attraction of the closed-loop system, i.e. the region in which initial states converge to the equilibrium, can not be determined, however. In the next section simulations are performed and it will be shown that in some cases this region of attraction can be quite large. For some heater heights it is not possible to stabilise the homogeneous transition boiling equilibrium and, although the observer state converges to the system state in those cases, the system state converges to a non-uniform (and therefore undesired) temperature profile.

4 Closed-loop Simulations

To determine the effectiveness of the control strategy discussed in the previous section, some simulations are done with the unstable transition towards film boiling is stabilised. It turns out that this transition state can only be stabilised for specific combinations of the heater properties λ (heater material) and L, H (heater dimensions), for given Q_H (nominal heat supply). This means that in the design of a thermal management system for EVs, it is important to determine the typical value for the heat generation Q_H and choose heater dimensions and material accordingly.
In the following, two case studies are discussed. The first represents the design of a cooling device for IGBTs and the second a thermal management and homogenisation scheme for a small battery cell. As the pressure can be varied only within a certain operating range, the input is restricted by $-0.8Q_H \leq u(t) \leq 2Q_H \; \forall \; t > 0$ in the simulations.

For the simulations, discretisation of the nonlinear system is accomplished by a Chebyshev-Fourier-cosine spectral method identical to that underlying (14) in combination with a second-order Cranck-Nicholson time-marching scheme [20]. This admits a highly accurate approximation of the underlying nonlinear PDE with reasonable finite resolutions. The discretised system is then solved for each Fourier-mode individually; their coupling via the boundary condition on $y = H$ is treated by a standard Picard iteration [19]. The initial conditions are constructed similarly as in [14]: $\widetilde{\mathbf{T}}(0) = \widetilde{\mathbf{T}}_\infty + \epsilon\mathbf{n}$, with $\widetilde{\mathbf{T}}_\infty$ the to-be-stabilised equilibrium and $\epsilon\mathbf{n}$ an exponentially-decaying Gaussian perturbation (standard deviation equals 1) with magnitude ϵ. In the following $\epsilon = 10^{-1}$ is taken.

4.1 IGBT-cooling

IGBTs are high-power switching devices used to switch large amounts of power from the battery pack to electrical coils, which produce about four times as much heat as a conventional computer chip. For this case study the heat generation Q_H is set to $Q_H = 15$ W/cm^2 see also [17]. For two different heater designs, i.e. the height of the heater is varied, the control strategy introduced above is applied to the system for stabilisation of the homogeneous transition state. It will be shown that the heater can not be made too thin as this promotes non-uniform temperature distributions in the device. The length of the heater in this case is $L = 80$mm, which is the length of an IGBT of dimensions 80×80mm.

4.1.1 Heater height: $H = 20$mm

The controller and observer parameters are taken according to

$$(k_{0,0}, k_{1,0}, k_{2,0}) = (-30, -10, 6.6), \quad q = 2, \tag{25}$$

and controller parameters for higher Fourier-Chebyshev modes, i.e. k_{nk} for $n > 3$ or $k > 0$, equal zero. In Fig.4 the simulated evolution of the interface temperature ($T_F(x,t) := T(x,H,t)$) is shown (progression in time is indicated by darker shades of grey of the intermediate profiles). This reveals a smooth progression from an essentially heterogeneous initial state, to the final homogeneous state. This means that disturbances that arise during operation can be suppressed effectively, resulting in constant and uniform temperatures. As can be seen the region of attraction is quite large in this case. Although the temperature of the IGBT is too high initially, the controller manages to remove the excess heat in the IGBT and the heater. As a result, the superheat drops to the desired value of 60K. Fig. 4 shows that the initial temperature fluctuations in x-direction are rapidly smoothed out, resulting in a homogeneous temperature distribution in the device.

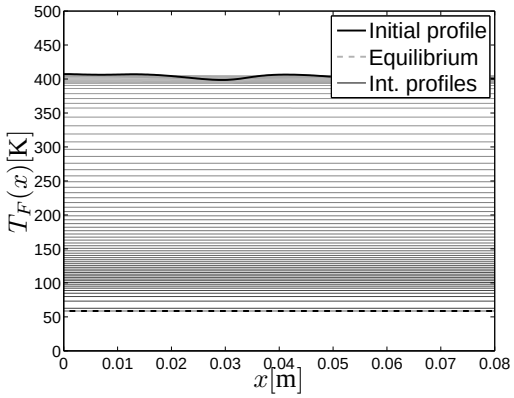

Figure 4: The evolution of the interface temperature $T_F(x,t)$ is shown for the IGBT-cooling case study, $H = 20$mm. The thin grey lines are intermediate profiles, progression in time is indicated by darker shades of grey.

The temperature as function of time in the points $(x,y) = (0,H)$, $(x,y) = (\frac{1}{2}L, H)$ and $(x,y) = (L,H)$, i.e. the validation points, of both system and observer is given in Fig. 5. It can be seen that the observer state quite rapidly converges to the system state, from whereon the system state converges to the equilibrium.

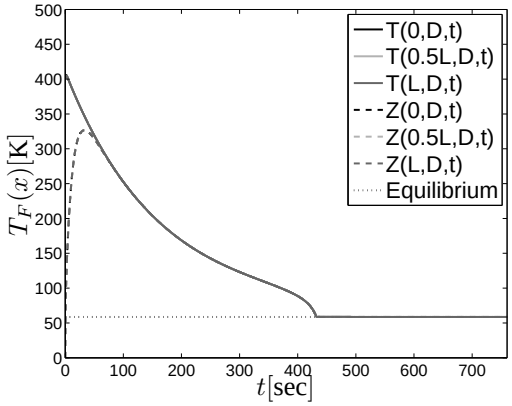

Figure 5: For the IGBT-cooling case study, $H = 20$mm, the evolution of the interface temperature of the system (solid line) and the observer (dashed line) are shown for $x = 0$, $x = \frac{1}{2}L$ and $x = L$.

Finally, the input used to stabilise the equilibrium is given as function of time in Fig. 6. Initially, the input is maximal due to the observers initial state, subsequently, the input is minimal until the temperature setpoint is reached.

4.1.2 Heater height: $H = 8$mm

If the heater is $H = 8$mm of height, the transition to film boiling can not be stabilised, since the interface temperature converges to a non-uniform

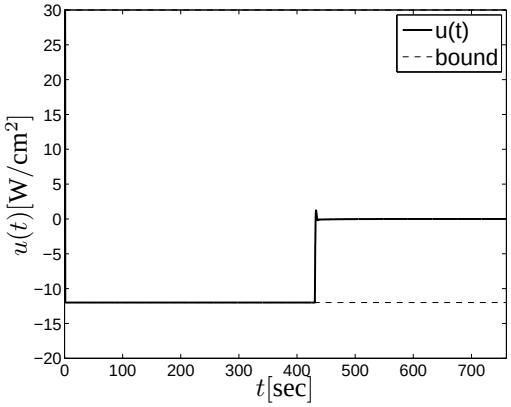

Figure 6: The input as function of time is shown for the IGBT-cooling case study, $H = 20$mm. The bounds of the input are given by the dashed lines.

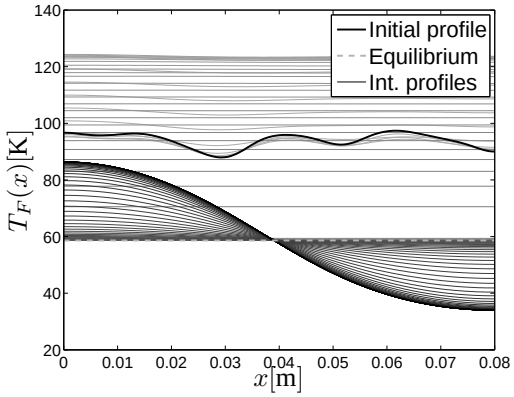

Figure 7: The evolution of the interface temperature $T_F(x,t)$ is shown for the IGBT-cooling case study, $H = 8$mm. The thin grey lines are intermediate profiles, progression in time is indicated by darker shades of grey.

state (partial vapour blanket). The controller and observer parameters are taken according to (25). The non-uniform state has temperatures that correspond to film boiling and regions with temperatures that correspond to nucleate boiling. The device thus will get very hot in some regions, while other regions still are well cooled. This phenomenon can not be avoided by taking different controller parameters as the homogeneous transition equilibrium is non-stabilisable for these system parameters. As the pressure can not be altered as function of x, the heat supply in our model must be varied uniformly. As a result, the system is not fully controllable. Depending on the system parameters the homogeneous transition equilibrium is then either stabilisable or non-stabilisable. In Fig. 7 the evolution of the fluid-heater interface temperature is shown. Although the initial condition is taken quite close the the equilibrium, the small perturbations are amplified by the boiling process resulting in the non-uniform temperature distribution. This results in a large temperature distribution in the device.

In Fig. 8 the evolution of the system and observer state in the validation points is given. Initially the observer state has a large deviation from the system state. As a result, the system state is regulated in opposite direction initially. After the observer state has converged on the system state, the system state is regulated towards the equilibrium. The non-uniformity thus is not the result of poor observer performance. After some time the system state starts to deviate from the equilibrium and convergence to a non-uniform state is observed.

In Fig. 9 the input as function of time is given. It can be seen that the input settles at a nonzero value after the system state has converged on the non-uniform state.

In some cases, the convergence on the non-uniform state can be remedied by varying the nominal pressure p (thus creating another equilibrium to stabilise). However, for these heater properties the only measure that can be taken, is a large safety margin between actual heat flux and

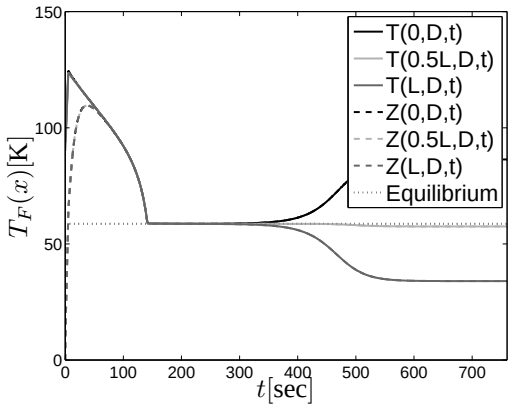

Figure 8: For the IGBT-cooling case study, $H = 8$mm, the evolution of the interface temperature of the system (solid line) and the observer (dashed line) are shown for $x = 0$, $x = \frac{1}{2}L$ and $x = L$.

critical heat flux (CHF). This will adversely affect the cooling efficiency, though.

4.2 Battery thermal management

The second case study is the thermal homogenisation of a small battery cell, like for example used in the Tesla Roadster. The same setup (Fig. 1) is used as thermal management scheme. Since the cells are closely packed together in a battery pack, the boiling chamber becomes very confined, thus significantly limiting the amount of boiling liquid. As a result, the net evaporation/condensation of the total amount of working fluid plays a significant role in the cooling process. Physical considerations suggest that in a first approximation this can be described by rescaling the boiling curve. The critical heat flux (CHF) will namely effectively decrease if

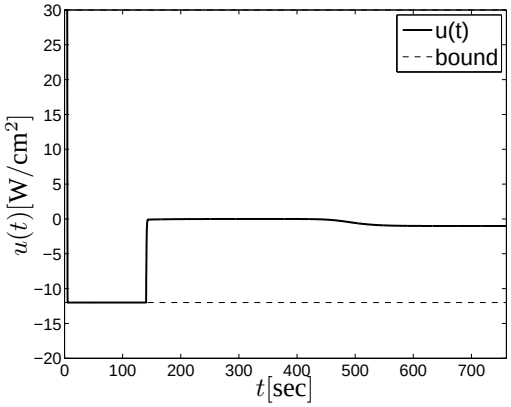

Figure 9: The input as function of time is shown for the IGBT-cooling case study, $H = 8$mm. The bounds of the input are given by the dashed lines.

the volume of the liquid phase of the boiling medium drops below a certain minimum due to net evaporation of the total amount of working fluid. For this case study the boiling curve given in Fig. 10 therefore is taken. The battery pack in the Tesla Roadster can deliver up to 200 kW of electric power at 95% efficiency, see [18]. This means the heat generation of an individual battery cell can be as high as approximately 0.33 W/cm^2. Hence, the heat generation is set to $Q_H = 0.33$W/cm^2 for this case study.

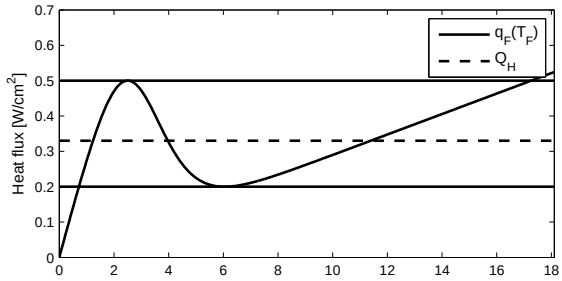

Figure 10: Nonlinear heat-flux function $q_F(T_F)$ according to the boiling curve of aluminum vs. FC-72, see [9]. The dashed line represents the nominal heat supply Q_H.

4.2.1 Heater height: $H = 3.5$mm

Controller and observer parameters are again according to (25). In Fig.11 the simulated evolution of the interface temperature ($T_F(x,t) := T(x,H,t)$) is shown (progression in time is again indicated by darker shades of grey of the intermediate profiles). Similar as for the IGBT cooling example an essentially heterogeneous initial state is regulated to the final homogeneous state. This means that disturbances that arise during operation can be suppressed effectively, resulting in constant and uniform temperatures in favour of a uniform temperature distribution throughout the battery pack. As can be seen, the region of attraction is quite large in this case as well. The too low initial temperature is increased by the controller by removing less heat from the battery. As a result, the battery warms itself until it reaches the desired temperature. The initial temperature fluctuations in x-direction are rapidly smoothed out, resulting in a homogeneous temperature distribution in the cell. This means temperature fluctuations can be smoothed very effectively by the thermal management scheme.

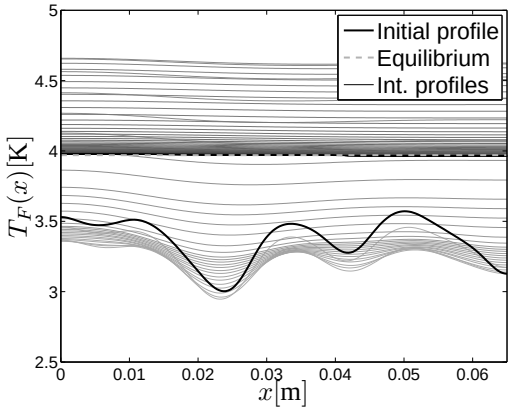

Figure 11: The evolution of the interface temperature $T_F(x,t)$ is shown for the battery-cooling case study, $H = 3.5$mm. The thin grey lines are intermediate profiles, progression in time is indicated by darker shades of grey.

The temperature as function of time in the validation points is given in Fig. 12. Again the observer state quite rapidly converges to the system state. Due to the initial error, the system overshoots its equilibrium value, however. After the observer state has reached the equilibrium the system state is regulated towards the equilibrium as well.

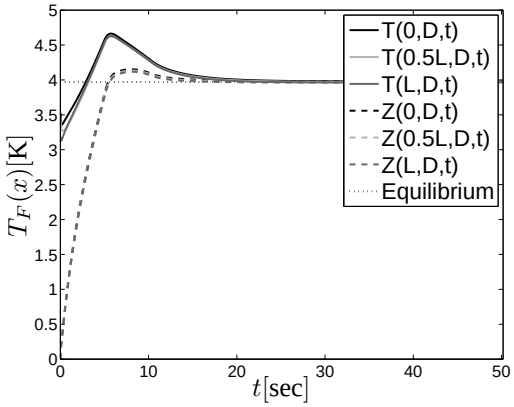

Figure 12: For the battery-cooling case study, $H = 3.5$mm, the evolution of the interface temperature of the system (solid line) and the observer (dashed line) are shown for $x = 0$, $x = \frac{1}{2}L$ and $x = L$.

Finally, the input used to stabilise the equilibrium is given as function of time in Fig. 13. Initially, the input is taken maximal, then minimal and subsequently it smoothly converges to zero as the system state converges on the equilibrium.

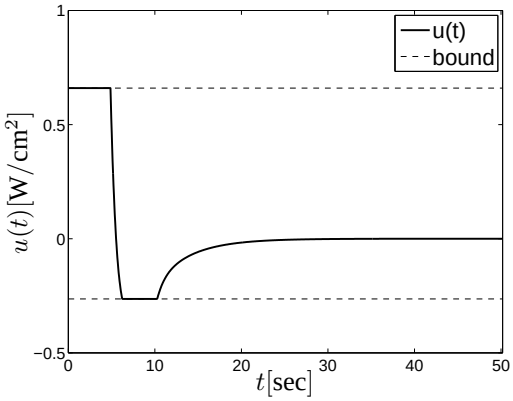

Figure 13: The input as function of time is shown for the battery-cooling case study, $H = 3.5$mm. The bounds of the input are given by the dashed lines.

4.2.2 Heater height: $H = 1.75$mm

If the heater is $H = 1.75$mm of height, the transition to film boiling can not be stabilised, since the interface temperature converges to a non-uniform state (partial vapour blanket). This represents a temperature non-uniformity in the battery cell, which is undesired. The controller parameters are taken according to (25). In Fig. 14 the evolution of the fluid-heater interface temperature is shown. Although the initial condition is taken quite close to the equilibrium, the small perturbations are amplified by the boiling process resulting in a non-uniform temperature distribution. As before, this can not be remedied by taking different controller parameters. Furthermore, the distributions represent local hot regions and local cold regions. Although the temperature non-uniformity does not exceed approximately 3K for this individual cell, it can accumulate to quite large differences in an entire battery pack.

Fig. 15 depicts the evolution of the system and observer state in the validation points. The figure shows that the non-uniformity is not the result of poor observer performance as the observer state converges to the system state quite rapidly. Furthermore, it can be seen that initially the controller keeps the system at its equilibrium, but then small fluctuations in x-direction are amplified and in the system converges to the non-uniform state.

In Fig. 16 the input as function of time is given. Again the input settles at a nonzero value due to the fact that the system has not converged on the equilibrium.

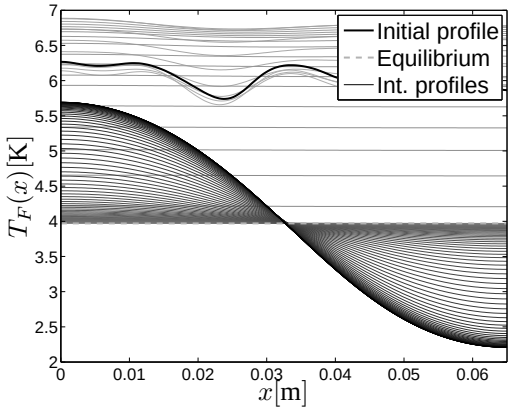

Figure 14: The evolution of the interface temperature $T_F(x,t)$ is shown for the battery-cooling case study, $H = 1.75$mm. The thin grey lines are intermediate profiles, progression in time is indicated by darker shades of grey.

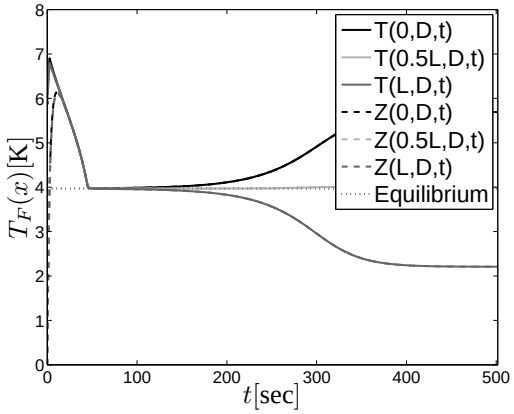

Figure 15: For the battery-cooling case study, $H = 1.75$mm, the evolution of the interface temperature of the system (solid line) and the observer (dashed line) are shown for $x = 0$, $x = \frac{1}{2}L$ and $x = L$.

5 Conclusion

In this study, a 2D nonlinear heat-transfer model for a boiling-based cooling device for cooling of Insulated Gate Bipolar Transistors (IGBTs) and battery thermal management in Electric Vehicles is considered. The model involves only the temperature distribution within the heater, i.e. a thermally conducting element between the to-be-cooled device and the boiling liquid. The heat exchange with the boiling medium is modelled via a nonlinear boundary condition imposed at the fluid-heater interface. In order to apply boiling at its fullest efficiency, unstable modes in the system must be stabilised.

To this end, a controller is introduced that regulates the pressure in the boiling system as a function of the heater temperature. by increasing (decreasing) the pressure, boiling can be sup-

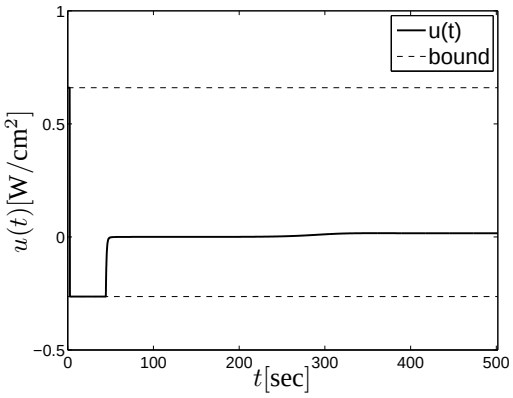

Figure 16: The input as function of time is shown for the battery-cooling case study, $H = 1.75$mm. The bounds of the input are given by the dashed lines.

pressed (stimulated) and as a result, more (less) heat can be extracted from the heater by the boiling liquid. In this way the boiling system can be kept in the efficient nucleate boiling regime. The entire temperature profile within the heater is estimated by an observer using only two measurements, both on top of the heater. Previous analyses have shown that controllers based on the dominant modes of the temperature profile within the heater are effective, see [16]. For this reason, the controller developed for this system is based on these modes as well.

The control strategy filters the Chebyshev-Fourier-cosine modes of the temperature profile of the heater. These modes are intimately related to the eigenmodes of the system. Therefore, the dynamics are mainly prescribed by the dominant modes, that is, the lower order Chebyshev-Fourier-cosine modes. The feedback law thus enables control of exactly those relevant lower order modes.

The observer is a copy of the nonlinear pool boiling model with an extra term in the boundary condition for the fluid heater interface, i.e. the top of the heater, by which convergence of the observer state on the system state is to be accomplished. This extra term accounts for the error between observer and system state on the fluid-heater interface.

Local asymptotic stability can be established via the linearised system and observer. Satisfactory closed-loop behaviour is obtained by fine-tuning of the control parameters using a characteristic equation which is derived using the method of separation of variables.

The performance of the control law for stabilisation of the nonlinear system is investigated in order to establish its value for practical purposes. Relevant issues are the asymptotic stability and evolution of the nonlinear closed-loop system. Simulations are performed for two case studies: (i) IGBT cooling and (ii) battery thermal management. It turns out that the closed-loop behaviour of the system is dependent on the system parameters such as height of the heater.

The first case study reveals convergence of the evolution of the nonlinear system on the unstable steady state for a wide range of initial states in case $H = 20$mm. These findings imply that the control loop indeed is capable of robustly stabilising the pool-boiling system for these parameters. For a thinner heater, $H = 8$mm, however, convergence of the nonlinear system on an essentially non-uniform state is observed. The final state has a region with temperatures corresponding to nucleate boiling ('cold spots') and has a region corresponding to film boiling ('hot spots'). This results in local 'hot-spots' on the IGBT and is highly undesired since it can lead to failure of the device. In some cases, this phenomenon can be remedied by varying the nominal pressure in the boiling chamber. However, for these heater properties the only measure is stabilisation of the nucleate boiling equilibrium. A safety margin needs to be taken into account for this measure, though, this affects the cooling efficiency negatively.

If boiling is applied to the individual cells in a battery pack, the net evaporation/condensation of the boiling liquid plays a significant role as the volume of the pool is much smaller due to the closely packed battery cells. Physical considerations suggest that this can in a first approximation be modelled by a rescaled boiling curve. Therefore, thermal management of these cells, in spite of their low heat generation, still is a challenge, since non-uniform temperatures and local 'hot spots' may still occur. The case study reveals that convergence to the unstable uniform transition boiling equilibrium can nonetheless be achieved for $H = 3.5$mm. For this case study, similar as for the IGBT-cooling case study, also convergence to a non-uniform state is observed for a thinner heater, i.e. $H = 1.75$mm. This is highly undesired in battery thermal management, as it leads to more rapid battery deterioration.

Nevertheless, both case studies show that the efficiency of boiling-based cooling schemes can be increased by dynamically varying the pressure inside the boiling chamber. This puts forth boiling heat transfer as a promising solution for thermal management issues in electric vehicles. During the design process heater material and dimensions must be chosen carefully, though.

Acknowledgements

This research is funded by the HTAS-REI (Range Extender Innovations) project.

References

[1] I. Besselink, J. Hereijgers, P. van Oorschot, and H. Nijmeijer, "Evaluation of 20000 km driven with a battery electric vehicle," in *Proc. EEVC*, (Brussels, Belgium), 2011.

[2] A. Pesaran, "Current and future needs in electric drive vehicle batteries," in *IHTC14*, (Washington DC), 2010.

[3] P. Ramadass *et al.*, "Capacity fade of sony 18650 cells cycled at elevated temperatures: Capacity fade analysis," *J. Power Sources*, vol. 112, pp. 614–620, 2002.

[4] A. Pesaran, A. Vlahinos, and S. Burch, "Thermal performance of EV and HEV battery modules and packs," in *Proc. 14th Int. EV Symp., Orlando*, 1997.

[5] R. van Gils, M. Speetjens, and H. Nijmeijer, "Boiling heat transfer in electric vehicles," Tech. Rep. DC 2011.52, Eindhoven U. of Tech., Dept. of Mech. Eng., 2011.

[6] H. van Ouwerkerk, "Burnout in pool boiling the stability of boiling mechanisms," *Int. J. Heat Mass Transfer*, vol. 15, no. 1, pp. 25–34, 1972.

[7] V. Dhir, "Boiling heat transfer," *Annu. Rev. Fluid Mech.*, vol. 30, pp. 365–401, 1998.

[8] I. Mudawar, "Assessment of high-heat-flux thermal management schemes," *IEEE Trans. Comp. Packaging Technol.*, vol. 24, no. 2, pp. 122–141, 2001.

[9] H. Auracher and W. Marquardt, "Heat transfer characteristics and mechanisms along entire boiling curves under steady-state and transient conditions," *Int. J. Heat Fluid Flow*, vol. 25, pp. 223–242, 2004.

[10] J. Blum, W. Marquardt, and H. Auracher, "Stability of boiling systems," *Int. J. Heat Mass Transfer*, vol. 39, no. 14, pp. 3021–3033, 1996.

[11] J. Blum *et al.*, "Temperature wave propagation as a route from nucleate to film boiling?," in *Proc. 2nd int. symp. two-ph. flow mod. and exp.*, (Rome, Italy), 1999.

[12] M. Speetjens, A. Reusken, and W. Marquardt, "Steady-state solutions in a nonlinear pool boiling model," *Com. Nonl. Sci. Num. Sim.*, vol. 13, pp. 1475–1494, 2008.

[13] M. Speetjens *et al.*, "Stability analysis of two-dimensional pool-boiling systems," *SIAM J. Applied Dyn. Sys.*, vol. 7, pp. 933–961, 2008.

[14] R. van Gils, M. Speetjens, and H. Nijmeijer, "Feedback stabilisation of a one-dimensional nonlinear pool-boiling system," *Int. J. Heat Mass Transfer*, vol. 53, pp. 2393–2403, May 2010.

[15] R. van Gils, M. Speetjens, and H. Nijmeijer, "Feedback stabilisation of a two-dimensional pool-boiling system by modal control," 2011. submitted for publication.

[16] R. van Gils, M. Speetjens, and H. Nijmeijer, "Feedback stabilisation of two-dimensional non-uniform pool-boiling states," in *Heat Transfer XI*, (Tallin, Estonia), pp. 215 – 226, WIT Press, 2010.

[17] R. Chu *et al.*, "Review of cooling technologies for computer products," *IEEE Trans. Device Materials Reliability*, vol. 4, pp. 568–585, 2004.

[18] G. Berdichevsky, K. Kelty, J. Straubel, and E. Toomre, "The tesla roadster battery system." Tesla Motors, August 16, 2006.

[19] E. Kreyszig, *Advanced Engineering Mathematics*. Wiley, New York, 1999.

[20] C. Canuto *et al.*, *Spectral Methods in Fluid Dynamics*. Springer, New York, 1987.

Authors

Rob van Gils received the M.Sc. degree (with great distinction) in Mechanical Engineering from Eindhoven University of Technology, in 2008. Since September 2008, he is a Ph.D. candidate with the Dynamics and Control group at the Mechanical Engineering Department of Eindhoven University of Technology.

Michel Speetjens received his PhD degree (with honours) in Applied Physics from Eindhoven University of Technology in 2001. During 2002-2005 he was postdoctoral researcher at CSIRO, Australia and RWTH-Aachen, Germany. Since 2006 he holds a position as assistant professor in thermal transport phenomena at Mechanical Engineering, Eindhoven University of Technology.

Henk Nijmeijer (1955) obtained his MSc-degree and PhD-degree in Mathematics from the University of Groningen, Groningen, the Netherlands, in 1979 and 1983, respectively. From 1983 untill 2000 he was affiliated with the Department of Applied Mathematics of the University of Twente, Enschede, the Netherlands. Since, 1997 he was also part-time affiliated with the Department of Mechanical Engineering of the Eindhoven University of Technology, Eindhoven, the Netherlands. Since 2000, he is a full professor at Eindhoven, and chairs the Dynamics and Control group.